

Parametric study of an active-passive system for cooling application in buildings improved with free cooling for enhanced solidification

E. Zavrl^{a,*}, U. Tomc^a, M. El Mankibi^b, M. Dovjak^c, U. Stritih^a

^a University of Ljubljana, Faculty of Mechanical Engineering, Ljubljana, Slovenia

^b National School of State Public Works (ENTPE), Vaulx-en-Velin, France

^c University of Ljubljana, Faculty of Civil and Geodetic Engineering, Ljubljana, Slovenia

ARTICLE INFO

Keywords:

Night ventilation
Phase change material
Thermal energy storage
Ventilated air gap
PCM integrated building elements
Computational fluid dynamics

ABSTRACT

The present study introduces an active-passive system (APS) with phase change material (PCM) integrated into the substructure of the internal walls and ceiling for cooling. To ensure sufficient cooling effect of the system during the daytime cycle, the system must solidify completely during the nighttime cycle and operation costs comparable to the ones of conventional cooling systems. An air gap was formed between the primary wall and ceiling and the PCM substructure and ventilated with the cool outdoor air during the nighttime cycle. A parametric study was performed using ANSYS Fluent followed by the energy performance and operation cost analysis. Different inlet air temperature scenarios (15–20 °C) were tested (suitable PCM thermal characteristics). The required solidification-time of PCM was determined. The model is validated against the experimental tests. The results show that with the current configuration, the PCM plates can be sufficiently solidified at supply air temperatures of 17 °C and below. If the system is ventilated with inlet air temperatures above 17 °C, additional cooling options must be considered. The study also determines the energy performance of the system under the chosen conditions and compares its feasibility to the conventional cooling systems (energy efficiency class A+++ and G air-conditioning device).

1. Introduction

Worldview, space heating and cooling are by final energy the two most important building activities and therefore, of crucial importance when it comes to reducing building emissions (space heating accounts for 45% of building emissions and 55% of final energy use is based on fossil fuels) (Abergel & Delmastro, 2020). It is estimated assumed the energy demand for cooling will in upcoming years increase (Statistical office of the European Union EUROSTAT, 2020; 'The Future of Cooling – Analysis - IEA', 2019; Delmastro et al., 2021; Isaac & van Vuuren, 2009).

Currently, most EU-recommended renovation measures focus on increasing thermal insulation of building envelopes and not buildings' thermal mass. Also, the recommended actions were to improve the

intelligence of air conditioning systems (AC), their flexibility and their ability to exploit synergies across services, and to develop renewable solutions to reduce cooling demand (Delmastro et al., 2021).

One of the most popular building concepts are certainly the lightweight buildings and buildings with large window areas. Due to the high heat reaction - low heat storage of the building - such buildings are easily overheated. This is especially a problem during the cooling season, when they need to be cooled immediately to ensure a comfortable and healthy living environment (Liu et al., 2017; Lomas & Porritt, 2017; Bundle et al., 2018). The topic of PCM, which is integrated into the transparent and non-transparent lightweight building envelope has been widely studied (Al-Yasiri & Szabó, 2023; Arkar et al., 2018; De Masi et al., 2020; Fateh et al., 2019; Duraković & Mešetović, 2019; Li et al., 2016; Li et al., 2018). It has been shown, that such integration improves indoor thermal

Abbreviations: AC, air-conditioning; ACH, air change per hour; APS, active-passive system; DO, discrete ordinates; DSC, differential scanning calorimetry; CIBSE, chartered institution of building services engineers; CSM, compact storage module; CV(RMSE), coefficient of variation of the root mean square error; EPBD, European directive on energy performance of buildings; ENTPE, national school of state public works; ESP, energy simulation program; HVAC, heating, ventilation and air-conditioning; IEA, international energy agency; IPCC, international panel for climate change; ISO, international standard organisation; NMBE, normalized mean bias error; OH, overheating; PCM, phase change material; R2, coefficient of determination; RANS, Reynold average Navier-stokes; TRY, test reference year; TRNSYS, transient system simulation tools; UDF, user defined function.

* Corresponding author.

E-mail address: eva.zavrl@fs.uni-lj.si (E. Zavrl).

<https://doi.org/10.1016/j.scs.2023.104960>

Received 10 July 2023; Received in revised form 1 September 2023; Accepted 24 September 2023

Available online 25 September 2023

2210-6707/© 2023 The Authors. Published by Elsevier Ltd. This is an open access article under the CC BY-NC license (<http://creativecommons.org/licenses/by-nc/4.0/>).

Nomenclature	
$A_{\text{air gap}}$	area of the air gap [m^2]
COP	coefficient of performance [/]
$c_{p, \text{air}}$	heat storage capacity of air [$\text{J}/(\text{kg}\cdot\text{K})$]
k	turbulence kinetic energy [m^2/s^2]
P_k	production of turbulent kinetic energy [m^2/s^2]
RH	relative humidity [%]
T_a	air temperature [$^{\circ}\text{C}$]
$T_{a, \text{cell}}$	mean air temperature measured in the centre of the cell [$^{\circ}\text{C}$]
$\Delta T_{a, \text{cell}} (0-5 \text{ h})$	temperature difference between the mean air temperature measured in the centre of the cell at the beginning and after 5 h of the case [$^{\circ}\text{C}$]
$\Delta T_{a, \text{cell}} (6-30 \text{ h})$	temperature difference between the mean air temperature measured in the centre of the cell after 6 h and after 30 h of the case [$^{\circ}\text{C}$]
T_{ai}	inlet air temperature [$^{\circ}\text{C}$]
T_{ao}	outlet air temperature [$^{\circ}\text{C}$]
T_m	PCM melting temperature [$^{\circ}\text{C}$]
T_{mr}	mean radiant temperature [$^{\circ}\text{C}$]
$T_{\text{PCM, back}}$	surface temperature measured on the front of the PCM plate [$^{\circ}\text{C}$]
$T_{\text{PCM, front}}$	surface temperature measured on the back of the PCM plate [$^{\circ}\text{C}$]
$T_{\text{PCM, back, avg}}$	average value of surface temperatures measured on the back of the PCM plate [$^{\circ}\text{C}$]
Q_s	heat stored for cooling [kWh]
ρ_{air}	air density [kg/m^3]
v	air velocity [m/s]
v_x	velocity of the air in x-direction [m/s]
v_y	velocity of the air in y-direction [m/s]
W_{in}	electrical energy [kWh]
Greek Symbols	
α	turbulent model coefficient [/]
β	turbulent model coefficient [/]
β^*	turbulent model coefficient [/]
β_T	thermal volume expansion coefficient [/]
λ	heat conductivity [$\text{W}/(\text{m}\cdot\text{K})$]
μ	dynamic viscosity [$\text{kg}/(\text{m}\cdot\text{s})$]
μ_{turb}	turbulent viscosity [$\text{kg}/(\text{m}\cdot\text{s})$]
ρ	density [kg/m^3]
σ_k	turbulent model coefficient [/]
σ_{ω}	turbulent model coefficient [/]
ω	specific dissipation rate [m^2/s^3]
Subscripts	
15–20 $^{\circ}\text{C}$	values measured at inlet temperature scenario of 15–20 $^{\circ}\text{C}$
1–13	values measured in PCM surface measuring points numbered 1–13
1–6	values measured in air-gap measuring points numbered 1–6
t_i	time at the beginning of the nighttime cycle (0 h) [h]
t_e	time at the end of the nighttime cycle [h]

comfort during the day by storing excess heat and thus lowering indoor temperatures (Zavrli et al., 2020; Ostry & Bečovský, 2009; Prabhakar et al., 2020; Agarwal & Prabhakar, 2023; Ahangari & Maerefat, 2019; Belmonte et al., 2015; Rathore et al., 2022).

During summer nights, however, PCM has difficulty solidifying completely. The thick layers of insulation prevent heat loss from the building and the heat stored in PCM is dissipated inward (Prabhakar et al., 2020). The air-based systems or systems which require air flow exploitation for their operation improve heat transfer during the night by increasing convective heat transfer from PCM to the air (Osterman et al., 2015; Abdo et al., 2020).

Such concepts of ventilated PCM improved building elements for cooling are in contact with horizontal and vertical air gaps. For example, on the outside of the building envelope, the ventilated PCM roof (horizontal air gap) was experimentally tested by Hou et al. (2021), in which two layers of PCM were separated by the air layer and ventilated by the wind (Hou et al., 2021). However, the PCM-improved roof is not practical for renovating only a single building space unit (e.g. office). In addition, while the wind does not consume electricity for ventilation, its absence during the solidification cycle makes the system unreliable. On the inner side of the building envelope, the ventilated PCM ceiling was numerically tested using TRNSYS by Lizana et al. where PCM was integrated into the suspended ceiling and ventilated (Lizana et al., 2019). While the advantages of using TRNSYS software are direct simulation with weather data and direct determination of energy use, the heat transfer calculation from air to PCM is less accurate compared to the one obtained with ANSYS software. The study shows the importance of local ventilation of the PCM layers, but the model is not validated alongside experimental results. Weinläder et al. positioned and monitored PCM panels in the suspended ceiling, with the panels in direct contact with the interior during the daily melting period and the ceiling gap ventilated overnight to accelerate nighttime solidification (Weinläder et al., 2014). The research is performed only under the experimental conditions, and it doesn't investigate other inlet temperatures. Furthermore,

the same concept was simulated by Jiao and Xu using Energy Plus (Jiao & Xu, 2015) which is compared to CFD tools less accurate for building-element-level heat transfer calculations.

Faheem et al. used ANSYS Fluent to numerically investigate the concrete slabs with addition of microencapsulated PCM (Faheem et al., 2016). The PCM improved concrete slabs are ventilated by circular hollow cores in them. Although microencapsulated PCMs are more suitable for use in load-bearing concrete elements, the amount of material is generally less compared to the macroencapsulated technique and therefore has less impact on thermal performance. Similarly, Yu et al. numerically investigated the ventilated hollow concrete slabs also using ANSYS software tool (Yu et al., 2020). However, compared to the previous study, PCM was not incorporated into the concrete, but was applied to the top of the slab as a PCM shape-stabilised layer. None of the last two studies performed a validation of the model by comparing numerical results to the experimental (Faheem et al., 2016; Yu et al., 2020).

Using Python 3.6, Morovat et al. tested an active PCM heat exchanger ceiling where a set of eight PCM plates were separated by ventilated air gaps (Morovat et al., 2019). While PCM is integrated into the suspended ceiling, the system works solely as an active heat exchanger and does not come into direct contact with the air in the room when it melts. However, the hollow horizontal building element can also be filled with PCM modules instead of the plates. Navarro et al. experimentally investigated the performance of a ventilated horizontal hollow ceiling designed primarily for the heating season (Navarro et al., 2016). Because the system is tested under the outdoor conditions it does not show the optimised results with parametric analysis. While an energy simulation program (ESP) can provide building heating and cooling loads with interior surface temperatures of building envelopes to CFD as boundary conditions, CFD can determine surface convective heat fluxes for ESP. In addition, CFD allows a more precise determination of Thermal comfort (Air temperature, air velocity airflow turbulence and air humidity), indoor air quality (contamination investigation) and air

distribution analysis.

The vertical building elements represent the interior and exterior walls. Evola et al. used Energy Plus to simulate the energy use of the building with the interior ventilated PCM wall (flow direction: top-bottom of the wall). The air gap formed by the space between the secondary PCM wall and the primary interior wall was ventilated during the night (Evola et al., 2014). Compared to CFD calculations, the heat transfers used in Energy Plus calculation aren't as accurate. Therefore, it is more challenging to determine the exact solidification time of the ventilated PCM wall.

However, compared to ventilated interior walls, there are more frequent examples of ventilated exterior walls (façades). For example, Gracia et al. studied the ventilated active façade, in which PCM plates were attached to the building façade, followed by the ventilated space and the external finish layer, which was naturally ventilated or ventilated by fans (De Gracia et al., 2013). Diarce et al. studied experimentally and numerically the ventilated façade with PCM using ANSYS Fluent. The exterior wall was followed by the mechanically upward ventilated air layer and the final layer of PCM plates with metal fins (Diarce et al., 2013; Diarce et al., 2014). While they successfully created a numerical model of the experiment, there was no further investigation of the influential parameters affecting the phase change of the material in the form of a parametric analysis. Also, the numerical model doesn't address the energy performance of the system. In addition, a rear-ventilated Trombe wall for active cooling and heating was mathematically studied by Zhou et al., where the wall consisted of two PCM layers: inside with embedded water pipes and outside in contact with the air layer and terminated by glazing as the last outer layer (Zhou et al., 2018). Even though the research shows a detailed calculation procedure, there is only one summer condition for inlet temperature investigated and is not validated compared to the experimental results.

Furthermore, Hu and Heiselberg used COMSOL Multiphysics to calculate a 2D model of a heat exchanger with PCM plates for summer cooling in Copenhagen, Denmark (Hu & Heiselberg, 2018). It investigates only one climate type scenario. In addition, Kant et al. studied a PCM layer on the BiPV wall and separated from the concrete wall by an air gap and calculated it using the COMSOL Multiphysics 5.0 software tool (Kant et al., 2019). Similarly, Li et al. created a 2D model of a double-skin glazing façade with laminated composite blinds PCM using the ANSYS Fluent software tool (Li et al., 2019). The numerical model was validated with smaller segment of the double-skin glazing. Despite the fact, that in the last two studies several different melting temperatures of the PCM were tested, only one (weather data) inlet air temperature was used (Kant et al., 2019; Li et al., 2019). The literature review by Zavr1 et al. presents and discusses the typical characteristics of ventilated PCM systems integrated in building elements for cooling application (E. Zavr1 et al., 2022).

It is visible from the literature review, that the topic of PCM in building envelopes for cooling application is prominent and a promising concept for passive urban cooling in cities, where the daily peaks in electrical energy demand for cooling are high (Han & Taylor, 2016; Mourid et al., 2018).

Therefore, the present study investigates the nighttime performance of the ventilated air gap in conjunction with PCM plates attached to the interior wall and ceiling for cooling. The main research objective is the investigation of the nighttime solidification cycle of the system with a parametric study performed with ANSYS Fluent 19.1. The results suggest the optimal PCM inlet air temperatures for the nightly PCM solidification in the air gap based on the outlet air temperatures and the average PCM wall surface temperatures validated by the experimental results. Also, the study shows the heat stored by the PCM plates and shows their maximum cooling potential. Compared to the systems with building elements improved with PCM on the external side of the building, the advantage of this system is that it can be used for the renovation of only a single building space unit (e.g. office). In this way, it can be used only where its application is necessary and feasible.

The research considers the following novelties:

- The novelty of the proposed system is the combination of a vertical ventilated PCM-improved building element (PCM -wall) with a horizontal one (PCM-ceiling) to achieve a maximum daily cooling effect.
- None of the studies present a full-scale (model is in the same size/scale as the experiment) validation of results obtained by the numerical model with the experimentally obtained results.
- While other similar studies investigate different melting temperatures of PCM, there are no variations in inlet air temperatures, which are crucial for determining the integral assessment of the thermal behaviour of the system. Despite the realistic values of the experimentally studied systems, the studies lack parametric analysis for optimal performance of the studied system. The case closest to full-scale validation was performed by Diarce et al. who did not perform any further parametric analysis to optimise the system (Diarce et al., 2014). Therefore, in reviewed studies, the question of the optimal inlet air temperature or the optimal PCM melting temperature selection often remained unanswered. Based on the last shortcomings, the novelty of this research is the parametric study of the PCM solidification time under different inlet air temperature scenarios. Especially, since the simulation model was challenged with the consideration of the effect of the variable environmental boundary conditions of the PCM plates in contact with the room air. Therefore, the system was not only defined by the adiabatic conditions on the air gap side of the PCM plates (actively ventilated), but also affected by the room side of the PCM plates (passively discharged).
- Additionally, most of the cited literature that use CFD methods assess the performance of the system based on the temperature distribution in building elements and offer no information on energy performance of the system (Faheem et al., 2016; Yu et al., 2020; Diarce et al., 2014; Li et al., 2019). Considering this fact, another novelty of this research is determining the energy performance of the system under the chosen conditions and comparing its feasibility to the conventional cooling systems (air-conditioning devices).

2. Method

2.1. Operation principle

The proposed diurnal PCM system for cooling consists of a passive (building systems that require no motive power, moving parts, or controls to function and are relatively low maintenance) and an active (building systems include mechanical systems for heating, cooling, and ventilation (HVAC), lighting, and control systems) operating cycle (Blumenfeld et al., 2014). Fig. 1 shows that during the daytime cycle, the system operates passively as the PCM plates melt and cool the indoor environment. During the night, the plates are actively solidified. The cool outdoor air is mechanically directed into the air gap through the linear diffuser at the bottom of the wall. The heated air (flow direction wall-ceiling) is mechanically exhausted through the ceiling exhaust. The arrows indicate the cool outdoor air (blue), the slightly heated air (yellow) and the hot air at the outlet (red).

2.2. Experiment

The numerical model was validated against the experimental results. The experimental case consists of a heating cycle and a cooling cycle. During the heating cycle, the inlet air temperature was set at 28 °C and the heating in the cell was adjusted to maintain the mean air temperature ($T_{a, cell}$) measured at the centre of the cell at 28 °C until the PCM plates were isothermally heated and the experimental conditions reached steady state. The room fan mixed the air in the cell at all times to melt the PCM plates more uniformly. During the cooling cycle, the

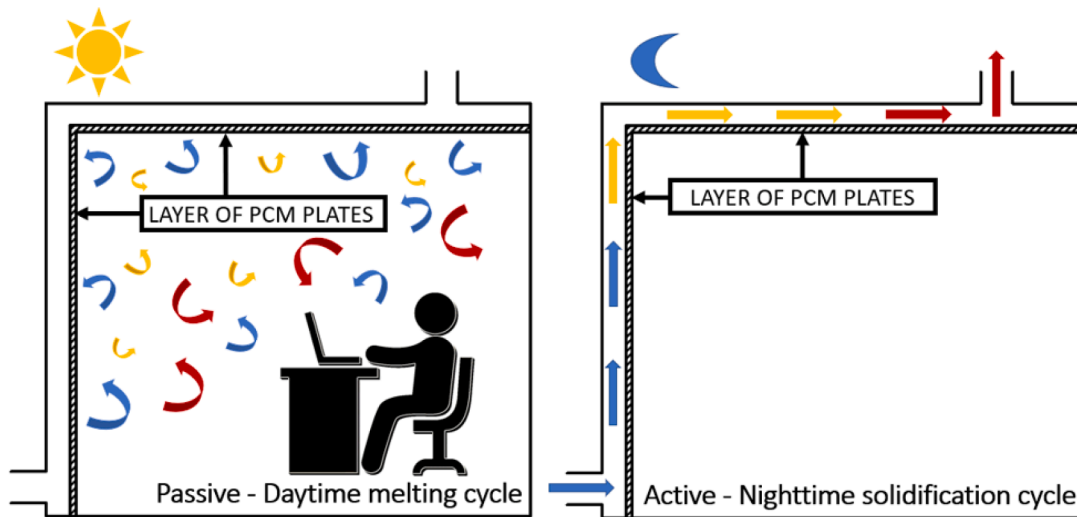


Fig. 1. The principle of diurnal PCM system: the daytime melting cycle (left) and the night-time solidification cycle (right).

heating was stopped after steady state was reached and the thermally conditioned cool air was blown into the air gap through the linear diffuser and then exhausted through the air gap outlet. The air gap was formed by the primary wall and ceiling of the cell and the 15 mm thick aluminium panels PCM filled with the product PCM Rubitherm SP 24 E and inserted into the wooden frame substructure of the experimental cell. The air gap was divided into five separate channels in the width of the PCM plate. Prior to testing, the air gap was tested for leaks using a smoke test. The experimental facility is named Hybcell and is located at the National School of Public Works (ENTPE) in Lyon, France (Fig. 2).

As shown in Figs. 2 and 3, inlet air temperature was measured directly at the two points of the linear diffuser (T_{a1} - T_{a2}). The outlet temperature was measured at four points around the outlet opening (T_{a3} - T_{a6}). Based on various air temperature combinations studied during the validation process, the average of the first two values was selected as the representative of the inlet air temperature (T_{ai}) and the average of the second four values was selected as the outlet air temperature (T_{ao}).

In addition to the air temperature measurement points (T_{a1} - T_{a6}),

Fig. 3 also shows 5 air velocity measurement points in the centre of the air gap channel (v_1 - v_5) and the 13 PCM surface temperature measurement points on the front (cell side; T_{PCM_front}) and back (air gap side; T_{PCM_back}) of the PCM plates on the wall and ceiling. The surface temperature sensor used were SFSC50 flexible temperature probe sensors with resistive element from C2AI (an uncertainty of $\pm 0.15\text{ }^\circ\text{C} + 0.002|T|$), the air temperature in the air gap was measured using sensor PT 100, both connected to DeltaOHM HD_35EDWH data acquisition. The mean air temperature in the cell ($T_{a, cell}$) was measured at the height of 1.1 m in the centre of the room with Wireless datalogging system: DeltaOHM HD_35EDG_1NB (accuracy: $\pm 0.2\text{ }^\circ\text{C}$, measuring range: 0–60 $^\circ\text{C}$). Velocities measured in each channel deviated from the mean by ± 0.4 m/s, indicating uneven flow distribution along the air gap. They were measured at the height of 1.3 m in the centre of each channel using DeltaOHM HD403TS and DeltaOHM HD4V3TS (accuracy: $\pm 0.05\text{ }^\circ\text{C}$, measuring range: 0.05–25 m/s and 0–40 m/s, respectively) anemometers (results shown in Fig. 6).

Fig. 4 shows the RTD surface temperature sensors and the sketch of

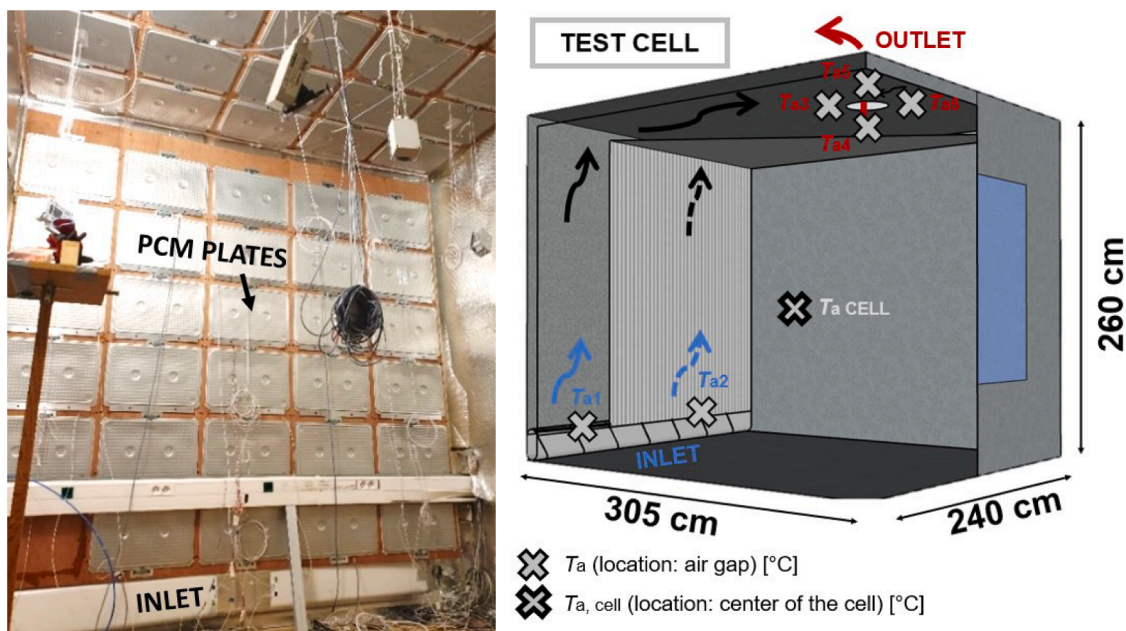


Fig. 2. The experimental test cell Hybcell (left) and the test cell inlet (T_{a1} and T_{a2}) and outlet (T_{a3} - T_{a6}) measuring points with test cell dimensions (right).

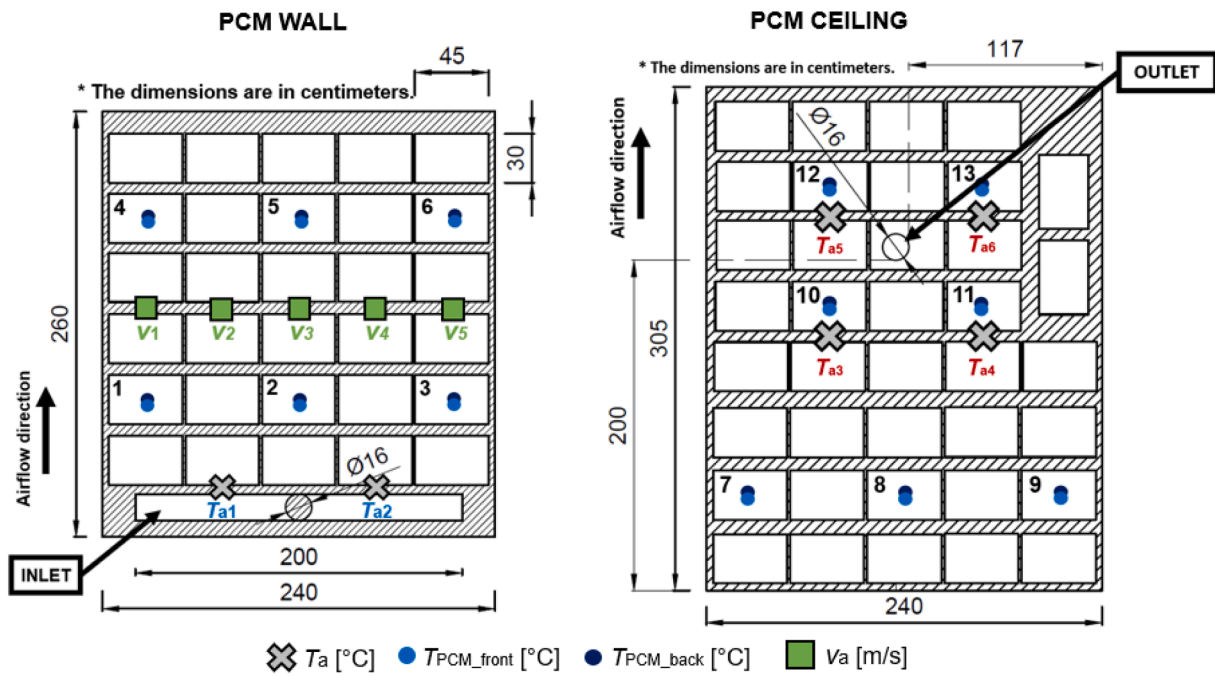


Fig. 3. The measuring points' locations on the PCM wall (left) and PCM ceiling (right).

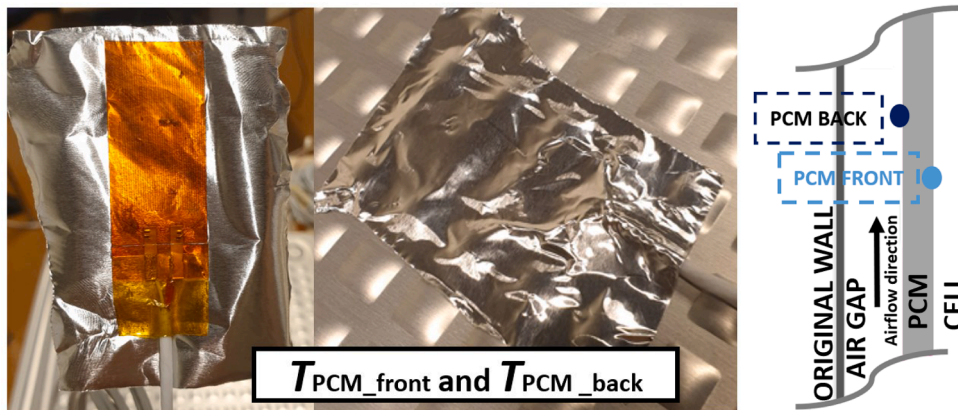


Fig. 4. RTD sensor attached to the PCM plate for of T_{PCM_front} and T_{PCM_back} temperature measurements.

the measuring points for the determination of T_{PCM_front} and T_{PCM_back} . The sensor was placed in the centre of the selected PCM plates at the same front and back point.

As a result, Fig. 5 shows the minimum, maximum and average T_{ai} , T_{ao} and T_{PCM_back} obtained in the experimental case, where the heated plates (28 °C) were cooled by the T_{ai} set at 16 °C. While T_{a1-2} and T_{a3-6} differ for up to 1 °C from their average values (T_{ai} and T_{ao}), it can be seen that the minimum and maximum T_{PCM_back} ($T_{PCM_back, 6}$ and $T_{PCM_back, 8}$) can differ from each other by more than 4 °C. The average surface temperature on the back side of the PCM plates ($T_{PCM_back, avg}$) was determined as the average of all 13 measured surface temperatures. More measurement results are presented in the study focusing on the experimental results (E. Zavr1 et al., 2022).

2.3. Input ansys fluent

2.3.1. General input

The purpose of this model is to evaluate the nocturnal (solidification) cycle. A simplified 2D model calculated using ANSYS Fluent v19.1 is proposed to calculate the air and PCM temperatures. The air flow in the

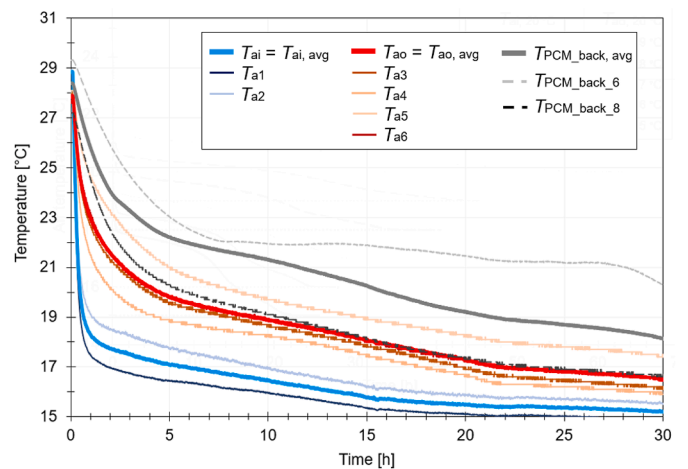


Fig. 5. The minimum, maximum and average T_{ai} , T_{ao} and T_{PCM_back} obtained in the experimental case.

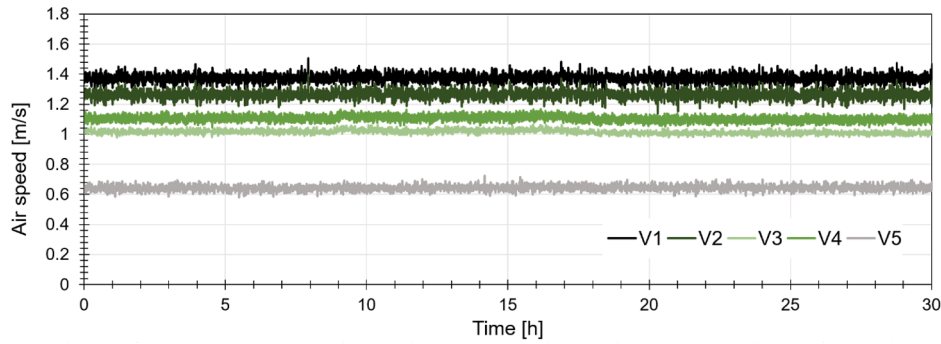


Fig. 6. Velocities measured in the centre of each channel of the air gap 1.3 m from the floor.

air gap is parallel to the edge of the PCM plates. This leads to the first assumption: the changes in z-axis may be neglected. The second assumption is, that the airflow distribution in the channel is uniform. The air gap is divided into 5 geometrical equal channels and the simulation plane is in the middle of the channel. The model is divided into two surface regions, the air gap (fluid region) and PCM (solid region). The unsteady model is calculated using ‘Energy model’ and the airflow in the air gap with standard viscous ‘model k- ω ’, which is suitable for the calculation of wall-bounded flows. K- ω was also confirmed by Diarce et al. as the best performing model for a ventilated air gap wall.

Transport equations for the standard k- ω model based on Reynold average Navier-Stokes (RANS) equations follow bellow Eqs. (1) and (2), where k – turbulence kinetic energy [m²/s²], ω – specific dissipation rate [m²/s³], P_k – generation of turbulent kinetic energy [m²/s²] and α , β , β^* , σ_k and σ_ω – turbulent model coefficients (Osterman, 2015).

$$\rho \frac{\partial k}{\partial t} + \rho \left(v_x \frac{\partial k}{\partial x} + v_y \frac{\partial k}{\partial y} \right) = P_k - \rho \beta^* k \omega + \frac{\partial}{\partial x} \left[\left(\mu + \frac{\mu_{\text{turb}}}{\sigma_k} \right) \frac{\partial k}{\partial x} \right] + \frac{\partial}{\partial y} \left[\left(\mu + \frac{\mu_{\text{turb}}}{\sigma_k} \right) \frac{\partial k}{\partial y} \right] \quad (1)$$

$$\rho \frac{\partial \omega}{\partial t} + \rho \left(v_x \frac{\partial \omega}{\partial x} + v_y \frac{\partial \omega}{\partial y} \right) = \alpha P_k \frac{\omega}{k} - \beta \omega^2 + \frac{\partial}{\partial x} \left[\left(\mu + \frac{\mu_{\text{turb}}}{\sigma_\omega} \right) \frac{\partial \omega}{\partial x} \right] + \frac{\partial}{\partial y} \left[\left(\mu + \frac{\mu_{\text{turb}}}{\sigma_\omega} \right) \frac{\partial \omega}{\partial y} \right] \quad (2)$$

Wilcox standard k- ω model assumes the following k- ω model constants to be: $\alpha = 0.52$, $\beta^* = 0.09$, $\beta = 0.072$ and $\sigma_k = \sigma_\omega = 2$.

Table 1
Calculation model assumptions.

Calculation model assumptions	
Air	PCM
<ul style="list-style-type: none"> The flow is defined incompressible (low airflow velocities) (White, 1998). The flow is transient/time dependant (Raj & Velraj, 2011). In the models, laminar and turbulent flows were simulated, depending on the simulation model’s geometry and airflow velocities (Munson et al., 2012). Air is defined as Newtonian fluid with constant density (except at fluids with volume force $\rho \vec{g}$ – Boussinesq approximation), specific heat, thermal conductivity and viscosity (Raj & Velraj, 2011). 	<ul style="list-style-type: none"> Heat transfer is obtained only by means of conduction (Rostamizadeh et al., 2012). Latent heat is released or absorbed in the temperature range of the phase change (Raj & Velraj, 2011). Phase change temperature is fixed, and it is the material property (Rostamizadeh et al., 2012). In the models, hysteresis was considered – only the characteristics of solidification part of the DSC diagram were used (Osterman, 2015). The material is homogeneous and isotropic (Rostamizadeh et al., 2012). The material properties such as density and thermal conductivity are the same for the solid and liquid phase (Raj & Velraj, 2011).

Table 1 shows the calculation model assumptions.

2.3.2. Model and boundary conditions

The model consists of the velocity inlet and outflow outlet. The primary wall has an adiabatic boundary condition and the PCM wall in contact with the indoor space (external PCM wall) the estimated temperature according to the investigated parametric scenario. The inlet velocity was set to 0.8 m/s and the initial PCM temperature to 28 °C, as measured during the experimental reference case. The fluid material air has a Boussinesq density of 1.18 kg/m³ and a coefficient of thermal expansion of 0.00336 1/K.

Boundary layer – air-PCM

The plate was formed by the aluminium case encapsulating the PCM. The thickness of the aluminium layer (red line) in contact with the ventilated air gap was 1 mm and it was neglected in the geometric model as shown in Fig. 7. In ANSYS Fluent model this boundary condition was generated as ‘Coupled’ which means that the heat transfer amongst two geometrical objects (zones: air and PCM) is enabled.

The calculation principle is shown in Eq. (3), where \vec{n} is the normal on the interface between air and PCM layer.

$$-\lambda_{\text{PCM}} \frac{\partial T}{\partial n} = \lambda_a \frac{\partial T}{\partial n}, T_{\text{PCM}} = T_a \quad (3)$$

2.3.3. PCM input

The PCM material investigated in this study is manufactured by Rubitherm. The PCM plates are originally encapsulated in the aluminium CSM cases. In the model, the thickness of the aluminium plates is neglected (0.65 mm) and the plates are simulated as a single unit (surface). The properties obtained from differential scanning calorimetry (DSC) are available on the product page (‘Rubitherm GmbH’, 2021). The salt hydrate SP24E with a melting temperature (T_m) and partial enthalpy of about 24 °C and 150 kJ/kg (Fig. 8) (Rubitherm, 2020). Due to hysteresis, the solidification of the material occurs at 22 °C and 23 °C with partial enthalpies of 118 kJ/kg and 42 kJ/kg, respectively. The material has a thermal conductivity (λ) of ~0.5 W/(mK) and a density (ρ) of 1500 kg/m³ and 1400 kg/m³ in the solid and liquid states, respectively. The material was selected based on thermal properties suitable for thermal comfort during hot summer periods in the cooling season in Ljubljana, Slovenia (EN 15251:2007:E, 2007).

Fig. 9 shows the material properties input inserted as a linear-



Fig. 7. The numerical simulation principle sketch of the air and PCM layer.

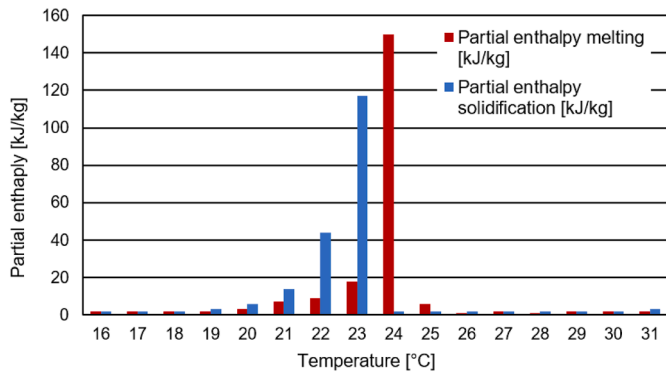


Fig. 8. DSC diagram rubitherm SP24E (Rubitherm, 2020).

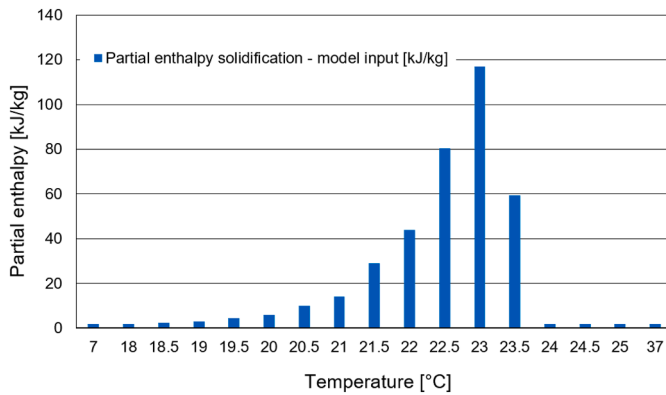


Fig. 9. Partial enthalpy in correlation with temperatures - numerical model input.

piecewise partial enthalpy in dependence of 17 temperature points.

The PCM was simulated as a solid material because the PCM wall is thin compared to the size of the system and convection in the slabs is assumed to be negligible, which significantly reduces the computation time compared to the fluid input with the melting and solidification model turned on. This approach was also confirmed in study by Diarce et al. (Diarce et al., 2014). The partial heat capacity of the material was inserted according to the corresponding temperature given in the DSC of the material by piecewise-linear option available in Fluent. The

thickness of the PCM layer (0.65 cm) was determined based on the mass weight of the PCM in the plate. The hysteresis was taken into account so that only the solidification properties of the DSC diagram were used in the material. The piecewise-linear option was also used for the density, which changed in relation to the temperature of the PCM material according to the linear fraction of its solid or liquid phase.

2.3.4. Geometrical model simplification

To avoid unnecessary geometric complexity and computational difficulties, the 3D model of the wall and ceiling is cut in the middle with a symmetry plane, where its intersection defines the 2D model geometry. So, the numerical outlet is positioned at the end of the air gap (Fig. 10). Due to the building structure of the laboratory such configuration was not possible in reality.

2.3.5. Parametric study

The parametric study examines the effects of an influential parameter - outdoor air inlet temperature (T_{ai}). Based on the nighttime outdoor air temperatures in south-central Europe (in this simulated case: Ljubljana, Slovenia), six different T_{ai} were selected (15 °C, 16 °C, 17 °C, 18 °C, 19 °C and 20 °C).

When the cooling cycle starts, the cell air is still heated and its effect on the calculation is not negligible. Two assumptions were made, one for the boundary condition temperatures at the PCM which is in contact with the cell air wall ($T_{PCM, front, avg}$), and the other for the calculation of the temperature at the PCM wall, which is in contact with the air gap ($T_{PCM, back, avg}$), which was presented in section '2.4 Validation'. First, the boundary on the front side of the PCM wall ($T_{PCM, front, avg}$) is in constant contact with the interior environment of the cell, which has a significant effect on the solidification process. This effect was measured in the experimental studies when PCM was solidified after the heating (melting) cycles. The air temperature was measured in the centre of the cell ($T_{a, cell}$) where the air was during the experiment mixed with the room ventilators.

Based on the experimental cases, the dynamics of cell temperatures during solidification were analysed. To test different T_{ai} , the boundary condition of the cell temperature $T_{a, cell}$ was extrapolated for each of the six parametric cases according to the experimental case below, with the initial PCM temperature of 28 °C and T_{ai} of 18 – 15 °C (Fig. 11). Similar dynamics of $T_{a, cell}$ decreases were observed in other experimental cases' measurements where the solidification cycle begins at 30 °C and are not presented within this article.

Table 2 shows the estimated air temperature differences in the cells for the corresponding constant T_{ai} scenario during two solidification

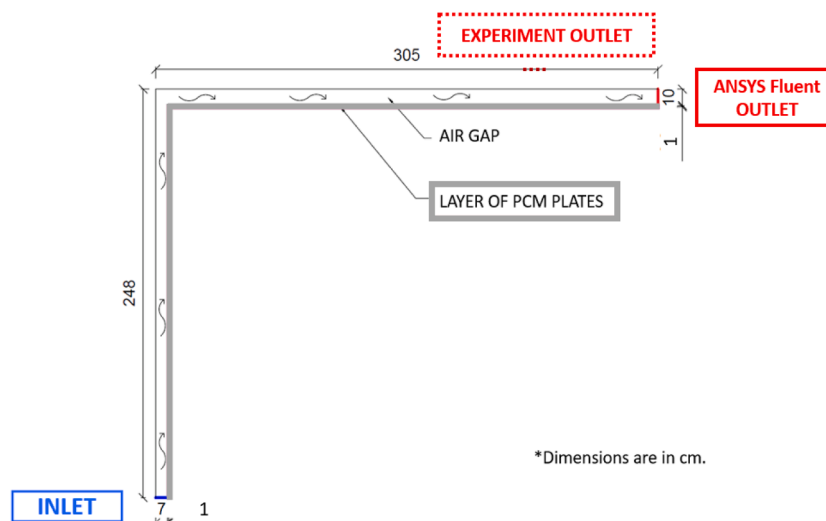


Fig. 10. Sketch of the 2D model of the airgap with PCM specification of the geometry simplifications.

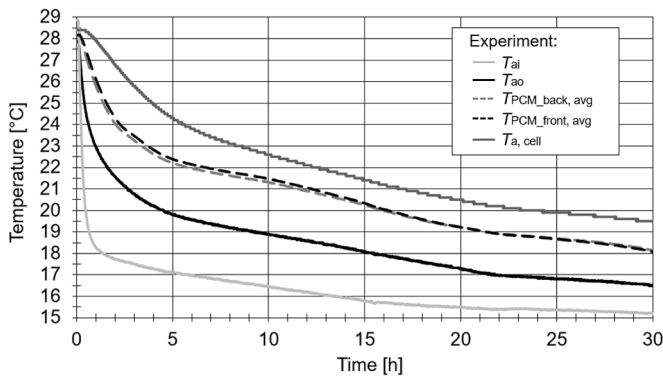


Fig. 11. Temperatures obtained during the reference experimental case in the cooling cycle.

Table 2

The estimated cell air temperature differences during two solidification periods for the determination of PCM wall boundary condition.

Inlet temperature scenario (T_{ai})	15 °C	16 °C	17 °C	18 °C	19 °C	20 °C
$\Delta T_{a,cell}$ (0–5 h)	3	3.5	4	4.5	5	5.5
$\Delta T_{a,cell}$ (6–30 h)	5	4.5	4	4.5	4	3.5

periods (the first 5 h and the second 25 h).

The curves presented in Fig. 12 are the estimated cell air temperatures during two solidification periods and inserted into the model via User Defined Functions (UDFs) as the PCM wall boundary condition for each case of inlet temperature (20–15 °C designated as $T_{a, cell}$, 20 °C - $T_{a, cell}$, 15 °C).

Both the T_{ao} and $T_{PCM, back, avg}$ are presented as area-weighted average areas. Unfortunately, the end of the phase change cannot be determined from T_{ao} alone because high ventilation rates of the supply air in the air gap prevent a visible end of the phase change curve. Therefore, the phase change cycles can be specified using $T_{PCM, back, avg}$. So, the time required for $T_{PCM, back, avg}$ to fall to 21 °C is the solidification time for each inlet temperature scenario. From the DSC diagram (Fig. 8), it can be seen that the PCM solidified at 21 °C.

During the validation process, the experimentally and numerically obtained $T_{PCM, back, avg}$ showed differences of more than 1 °C, which strongly affected the solidification time determination. It was concluded that the effect of the directly inserted experimentally measured $T_{a, cell}$ were not suitable for the model's $T_{PCM, front, avg}$ boundary condition. The numerical $T_{PCM, back, avg}$ values were brought closer to experimental by observing other experimental results. As visible from Fig. 13, the

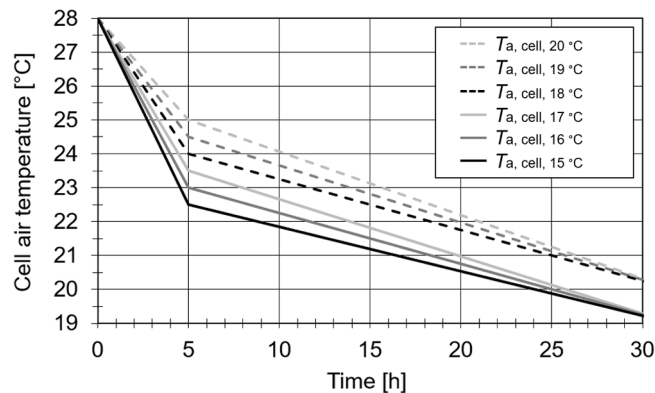


Fig. 12. The estimated cell air temperatures during two solidification periods for the determination of PCM wall boundary condition.

average temperature difference between $T_{PCM, front, avg}$ and $T_{a, cell}$ among four other experimental cases was 0.8 °C (± 0.4 °C). Therefore, the individual case of $T_{a, cell}$ temperatures were subtracted for 0.8 °C and inserted as boundary condition for $T_{PCM, front, avg}$.

2.4. Validation

2.4.1. Validation of numerical model with experimental data

For the purpose of validation, two cases were studied. Table 3 shows the validation analysis of both types of validation of numerical model with experimental data.

First, a special validation case was measured in which a complete melting/solidification cycle was studied. Fig. 14 shows and describes the 1st validation set up. In this case, the plates are melted and solidified only by the heated or cooled inlet air. Both phases, melting and solidification, of PCM were studied considering the hysteresis of the material (the properties of PCM (melting/solidification temperature and partial enthalpy) were adopted according to the heating or cooling period) (Fig. 15).

The errors, Normalized Mean Bias Error (NMBE), Coefficient of Variation of the Root Mean Square Error (CV(RMSE)) and coefficient of determination (R^2) are NMBE = -0.096%, CV (RMSE) = 2.749% and $R^2 = 2.051\%$ ($R^2 = 0.979$) are calculated according to Ruiz and Bandera (2017).

Second, the reference experimental solidification case was closely examined also for $T_{PCM, back, avg}$. Fig. 16 shows and describes the 2nd validation set up.

The results show that the trend of the simulated T_{ao} and $T_{PCM, back, avg}$ temperatures drop correlate with the measured ones, even though the simulated T_{ao} and $T_{PCM, back, avg}$ temperatures deviate from the experimental values for up to 1 °C (Fig. 17). The following errors NMBE = 3.2292%, CV(RMSE) = 3.852% and $R^2 = 2.299\%$ ($R^2 = 0.979$) were determined and calculated according to Ruiz and Bandera (2017).

On one hand, this could be due to the experimental errors, such as the uneven phase transition along the PCM wall and ceiling and the other side was in contact with the ambient air, possible minor air leaks in the air gap and heat transfer losses through the original wall and ceiling (even though they are both insulated, in nature this is layer doesn't present and adiabatic boundary condition). Also, the air measured air velocity might still differ from the simulated one as it was determined based on the average of five measured points in the air gap. On the other hand, numerical errors may arise due to assumptions and model simplifications. For example, an effect of $T_{a, cell}$ applied to the PCM wall boundary condition could be too significant. Due to mixing of the cell air, the temperature distribution along the PCM wall and ceiling was considered uniform (in nature, the same temperature did not appear simultaneously near the wall and ceiling). Also, in the air gap no radiation calculation models were considered.

Considering the temperature differences along the PCM wall and ceiling and the scale of the experiment (room level), the temperature difference of 1–2 °C between the experimental and numerical results is considered acceptable. Accordingly, also other authors showed discrepancies between the results of experiments and numerical calculations during nighttime solidification times in the presence of ventilation in active air-based systems with PCM for cooling application modelled at the level of a building element.

For example, Diarce et al. reported a mean temperature error between experiment and numerical calculation based on the outlet air and PCM material on the wall in front of the outlet of 1.0–2.23 °C and 1.34–2.50 °C, respectively (Diarce et al., 2014). Faheem et al. also showed a surface temperature difference at the bottom of the slab of ± 1.25 °C (Faheem et al., 2016). Hu and Heiselberg observed the outlet air temperature from experimental and numerical results and found a deviation of 2 °C between 3.5–5.5 h of ventilation period (Hu & Heiselberg, 2018). Kant et al. compared the measured and calculated PV temperatures and found a temperature difference of 2–6 °C (Kant et al.,

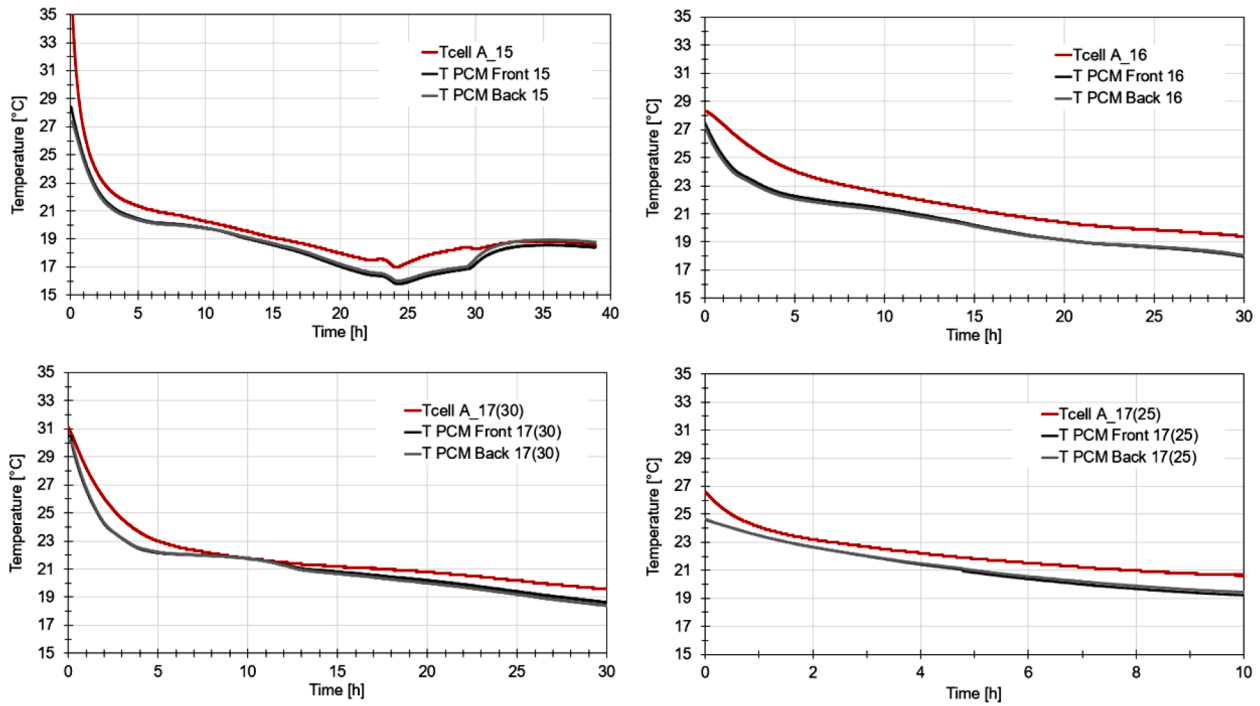


Fig. 13. Experimental cases showing the characteristic temperature difference between $T_{PCM, front, avg}$ and $T_{a, cell}$.

2019). However, Li et al. observed the profiles of the average air gap air temperature along the height of the double-glazed façade with PCM, where the simulated values differed by 1.5 °C from experimental ones (Li et al., 2019).

2.4.2. Grid and time step independence tests

Figs. 18 and 19 show the test of grid and time step independence test based on the outlet air temperatures (T_{ao}) and PCM surface temperatures $T_{PCM, back, avg}$ during 25 h of operation, respectively. The results are based on the tested grid size (2 mm, 5 mm, 10 mm, 15 mm and PCM /air gap: 10 mm/20 mm) and time steps 10 s, 30 s and 120 s. Some of the lines from 2 mm (10 s) to 10 mm (30 s) may be less visible, due to overlapping.

The statistics prove that the numerical results obtained with the 10 mm grid and time step of 30 s are consistent with the 2 mm grid and time step of 10 s. The model was simulated with 5 mm grid with 21,004 grid elements (grid in Fig. 20). The numerical validation follows the experimental results, where the sampling rate was set to 30 s. Therefore, the time step in the numerical model is fixed accordingly (30 s).

By considering $y=30$ and other parameters as they are defined within this manuscript, the calculated height of the first row of grid cells was $y = 9.7$ mm ('Fluent 13.0 Lecture06-Turbulence Near Wall | PDF | Reynolds Number | Turbulence', 2023). The grid used within this model is smaller (5 mm) than the calculated y . Therefore, it was considered that the use of inflation is not required.

2.5. Heat stored for cooling

In Eq. (4), heat stored for cooling Q_s is determined with area of the air gap $A_{air\ gap} = 0.168\ m^2$, density of air $\rho_{air} = 1.188\ \frac{kg}{m^3}$, heat capacity of air $c_{p, air} = 1.007\ \frac{kJ}{kg \cdot K}$, air velocity $v = 0.8\ \frac{m}{s}$, inlet air temperature T_{ai} , outlet air temperature T_{ao} , time at the beginning of the nighttime cycle $t_i = 0\ h$ and time at the end of the nighttime cycle (when the PCM is solidified) t_e .

$$Q_s = A_{air\ gap} \cdot \rho_{air} \cdot c_{p, air} \cdot \int_{t_i}^{t_e} v \cdot (T_{ao} - T_{ai}) \cdot dt \quad (4)$$

2.6. Energy performance and operation costs

As stated in Introduction, the advantage of the proposed APS in this study is that it may be utilized in the renovation of only a single building space unit (e.g. office). However, usually a convenient, fast and relatively inexpensive approach to tackle the issues of cooling of a single space unit would be to install the air conditioning device. Therefore, a question arises whether or not the application of the proposed APS could be a viable solution in comparison to classical air conditioners. Two aspects need to be addressed, energy use as well as the operation cost of a particular cooling system.

According to Eq. (4), the proposed APS is able to store 6.34 kWh of cooling energy, which may be utilized for cooling purposes during daytime. To store the said amount of cooling energy the ventilation has to consume 2.52 kWh of electrical energy during nighttime (two air fans EXTHCAS 200-4, each providing 101 m³/h at 0.18 kW input power ('Ventilateur Centrifuge mobile/chantier, mono/triphasé -Ventilation VIF', 2022)).

According to Commission Regulation (EU) No 626/2011 supplementing Directive 2010/30/EU of the European Parliament (European Council, 2011) the air conditioners with cooling capacities below 12 kW are classified in several energy efficiency classes. The Directive defines the energy classes going from A+++ (most efficient) to G (least efficient). As shown in European Council (2011) the A+++ class should have a seasonal COP 5.1 or higher, while the G class should have the seasonal COP 1.9 or lower. In such manner and according to the following equation, we can determine how much electrical energy (W_{in}) would an air conditioner of a particular class need to consume to run the compressor and to produce equivalent cooling energy of 6.34 kWh (Eq. (5)):

$$W_{in} = \frac{Q_s}{COP} \quad (5)$$

Table 3
Validation of numerical model with experimental data analysis.

	1st validation	2nd validation
Validation purpose	The purpose of this validation is to test PCM characteristics input in ANSYS Fluent and to understand whether the model's phase change dynamics respond equally to the experimentally measured phase change.	The purpose of this validation is to compare the vital target results of both investigations and see whether the thermal response of the numerical model represents the relevant experimental behaviour.
Description of the set up	In this case, the plates were preheated to 25 °C. During the first period (0–19 h), the air gap was ventilated with cool air (Experimentally obtained inlet air temperature fluctuations (T_{ai}) were used also in the numerical model and inserted via UDF function). In the second period (19–60 h), the spiral heater in the supply duct heated the air (increased T_{ai}) which was through the linear diffuser at the beginning of the air gap blown into the air gap. It has to be noted that, the heated air in the air gap was the only heat source for PCM plates melting and the heat source in the test cell was switched off. In the last period (60–93 h), the plates were again solidified with cool T_{ai} (Fig. 14).	The second validation presents the solidification cycle of the plates preheated to 28 °C. The plates are cooled only by the ventilation in the air gap with cool T_{ai} . The validation period shows the first 30 h of solidification case. The presented T_{ai} were measured experimentally and used also in the numerical model and inserted via UDF function (Fig. 16).
PCM thermal characteristics input	During the simulations, where both, heating and cooling cycles were simulated, the partial enthalpies were averaged for each temperature of DSC.	During the simulations where only the cooling cycle was simulated, the partial enthalpies were obtained only from the cooling segment of the DSC diagram. Additionally, the cooling enthalpy input was linearly interpolated between two neighbouring temperatures to enable a more accurate and smooth iteration process (Fig. 9).
Evaluation of the errors	The errors between the experimental and numerical results are determined based on the entire period shown in the graph (0–93 h). The errors are: <ul style="list-style-type: none"> • NMBE = -0.096% • CV (RMSE) = 2.749% • R2 = 2.051% (R2 = 0.979) 	The errors between the experimental and numerical results are determined based on the entire period shown in the graph (0–30 h). The errors are: <ul style="list-style-type: none"> • NMBE = -3.2292% • CV (RMSE) = 3.852% • R2 = 2.299% (R2 = 0.979)
Compared parameter	T_{ao} (exp) to T_{ao} (Fluent)	<ul style="list-style-type: none"> • T_{ao} (exp) to T_{ao} (Fluent) • $T_{PCM,back, avg}$ (exp) to $T_{PCM,back, avg}$ (Fluent)
Description of graph by segments	Three segments (T_{ao}) are presented in Fig. 15: <ul style="list-style-type: none"> • First period (0–19 h): The numerical T_{ao} (Fluent) curve is neglectable higher (+0.2 °C) compared to T_{ao} (exp). • Second period (19–60 h): In the first 3 h, the T_{ao} (Fluent) is considerably higher (up to +2.0 °C) with a peak compared to T_{ao} 	Two segments (T_{ao}) are presented in Fig. 17: The numerically obtained temperatures T_{ao} (Fluent) are lower (-0.3–2.1 °C) compared to T_{ao} (exp). <ul style="list-style-type: none"> • The largest difference occurs after 2 h. Afterwards, the difference stays at around +0.5 °C. • The trend between the curves matches.

Table 3 (continued)

	1st validation	2nd validation
	(exp). However, the trends of the curves match. In the next 58 h, the T_{ao} (Fluent) from +0.2 °C difference stabilizes and completely meets T_{ao} (exp). <ul style="list-style-type: none"> • Third period (60–93 h): During the final solidification period, in the first 3 h the T_{ao} (Fluent) drops below T_{ao} (exp) (up to -2.0 °C) and afterwards – in the next 10 h equalizes the trend with T_{ao} (exp) and meets its values. Some relevant temperature deviations occurred. Especially in the last period, seems that in the experiment additional thermal mass was present (such as primary wall and ceiling, which are adiabatic boundary conditions in numerical model). Also, the deviation may occur due to experimental system imperfections, such as air leakage. However, on the room-level, the deviation is considered acceptable. 	On the room-level, the deviation is considered acceptable. It seems that the thermal mass in the experiment was higher compared to the mass in numerical model. In numerical model there are some adiabatic conditions, while in reality the system is attached to the primary wall and ceiling. Similar temperature deviations were observed in other studies performing validation on the room-level. Also, the deviation may occur due to experimental system imperfections, such as air leakage. Two segments ($T_{PCM,back, avg}$) are presented in Fig. 17: <ul style="list-style-type: none"> • First period (0–10 h): First, the $T_{PCM,back, avg}$ (Fluent) temperature fluctuates higher (up to +1.0 °C; peak at 5 h) compared to the $T_{PCM,back, avg}$ (exp). • Second period (10–30 h): Afterwards, the $T_{PCM,back, avg}$ (Fluent) meets the $T_{PCM,back, avg}$ (exp) values. On the room-level, the deviation is considered acceptable. Similar temperature deviations were observed in other studies performing validation on the room-level. It has to be noted, that the $T_{PCM,back, avg}$ (exp) curve is an average value of all 13 measuring points on the PCM wall and ceiling where the largest difference among them ($T_{PCM,back,6}$ and $T_{PCM,back,8}$) is 4.1 °C.

3. Results

3.1. Determination of solidification time based on the temperature distribution in adiabatic conditions

The purpose of calculating the solidification cycle in adiabatic conditions is to see the behaviour of the material without other boundary conditions and to further on based on the outlet air temperatures T_{ao} evaluate the energy released from the PCM during the solidification period. Fig. 21 shows outlet air temperatures obtained in adiabatic conditions for different inlet air temperature scenarios.

The results show that the complete solidification with higher inlet temperatures takes up to 60 h (20 °C) and at lower (15 °C) at least 21 h. Of course, this amount of time may seem too long to consider the use of this PCM plates in the building. However, it must be noted, that under these circumstances, the goal is to discharge the material to the inlet air temperature which requires a large amount of time. Especially, because there is no thermal losses to the environment as they appear with a building application.

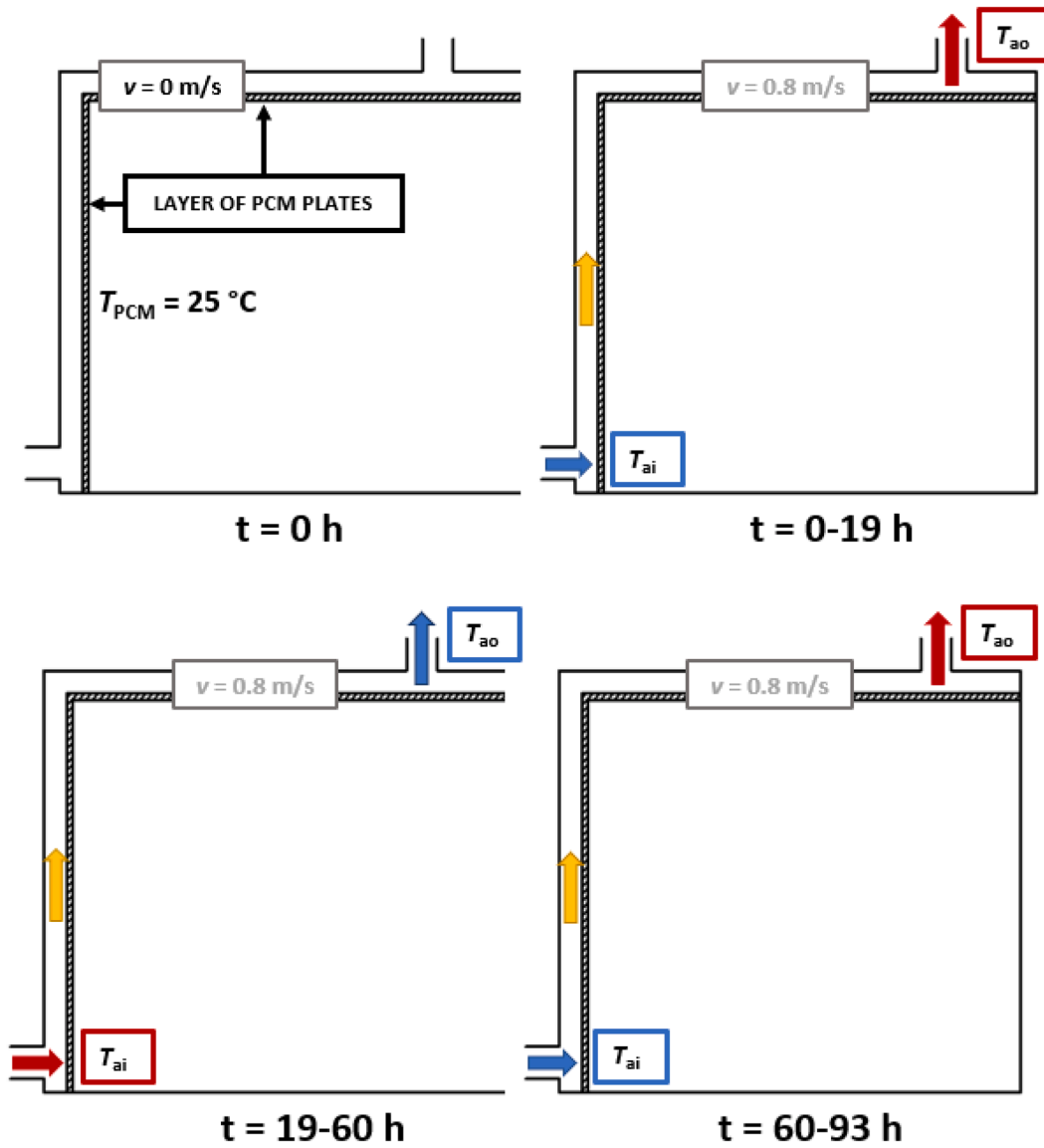


Fig. 14. Description of the 1st validation set up.

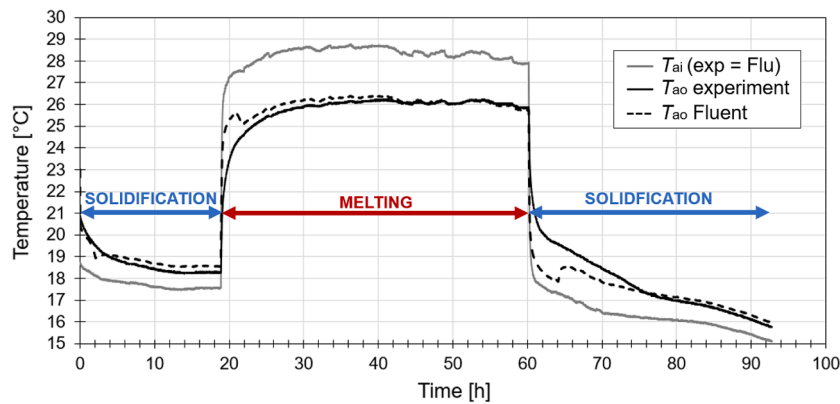


Fig. 15. The first validation case (melting/solidification) based on the outlet air temperatures.

3.2. Determination of solidification time based on the temperature distribution during each inlet temperature scenario

The time required for the surface temperature measured at the front

of the PCM plate ($T_{\text{PCM_back, avg}}$) material temperatures to drop to $21 \text{ }^\circ\text{C}$ is considered the solidification time for each inlet temperature scenario. The results show the temperatures obtained during the cooling cycles for each inlet temperature scenario. The figures show that the solidification

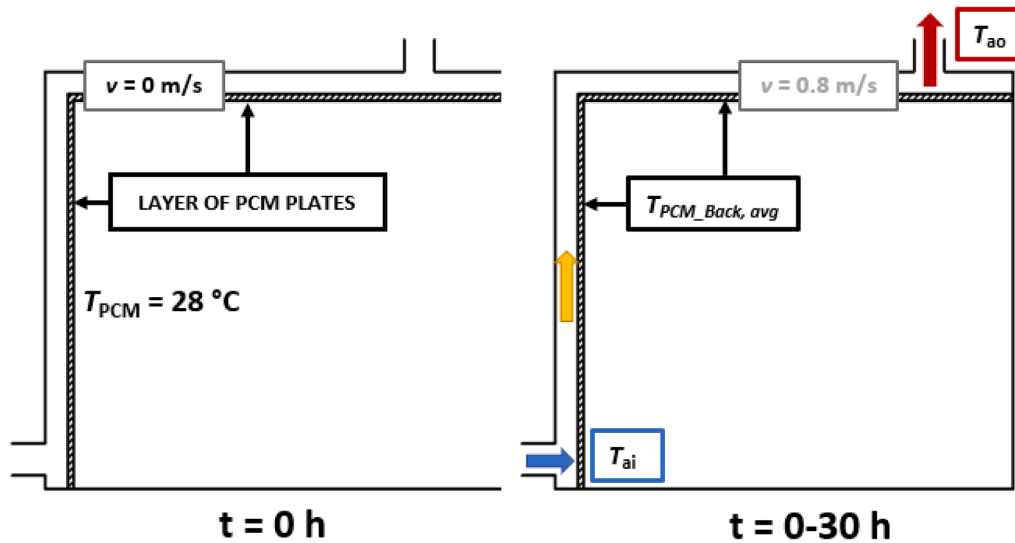


Fig. 16. Description of the 2nd validation set up.

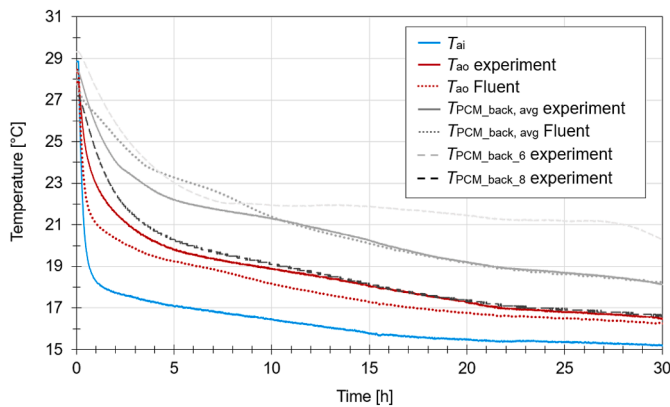


Fig. 17. The second validation case (solidification) – based on the outlet air temperatures and average surface PCM temperature (back).

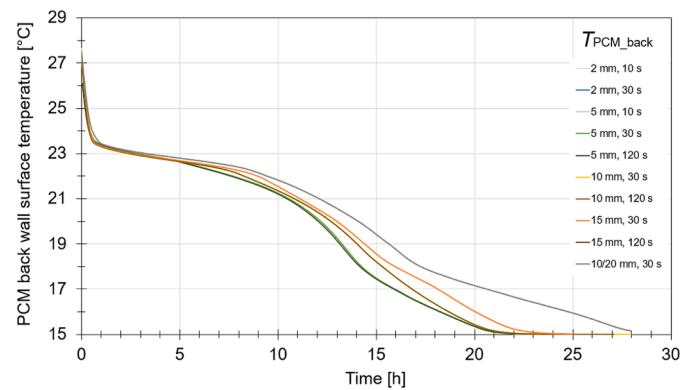


Fig. 19. Grid and time step independence test of PCM surface temperatures $T_{PCM_back, avg}$ during 25 h of operation (note: the lines from 2 mm (10 s) to 10 mm (30 s) are overlapping).

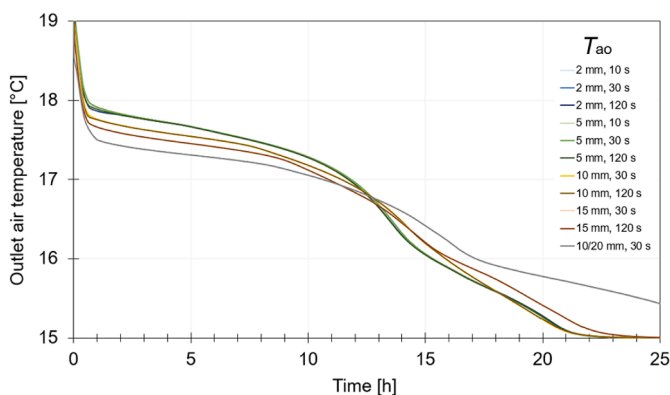


Fig. 18. Grid and time step independence test of Outlet air temperatures T_{ao} during 25 h of operation (note: the lines from 2 mm (10 s) to 10 mm (30 s) are overlapping).

is completed in a nighttime cycle only when the inlet air is supplied at 15 °C and 16 °C and almost at 17 °C. In Figures Figs. 22–24, the horizontal and vertical red dotted lines represent the temperature limit of 21 °C and the end of the nighttime cycle at 12 h, respectively.

Fig. 22 shows the results obtained when the inlet air temperature

(T_{ai}) was 15 °C. The average surface PCM temperatures (Back) dropped to 20 °C in the first 12 h and to 18 °C in 30 h. This shows that on average the PCM material completely solidified during the night.

Fig. 23 shows the results obtained at the inlet temperature of 16 °C. The average surface PCM temperatures (Back) decreased to 20.5 °C in the first 12 h and to 18 °C during the entire simulation period (30 h).

Fig. 24 shows that at the inlet temperature of 17 °C, the average surface PCM temperatures (Back) dropped to 21 °C in the first 12 h and to 18 °C during the entire simulation period (30 h).

3.3. Determination of energy released from PCM during the solidification period in adiabatic conditions

The following chapter presents the energy released from the PCM plates (Q_s) calculated based on the outlet air temperatures obtained in adiabatic conditions for different inlet air temperature scenarios (following Eq. (2)) and compared to the theoretically determined total heat storage capacity of the plates in the temperature range defined in Fig. 8. It was determined that 68 plates can store 6.53 kWh of energy. The deviation was calculated based on the subtraction of the of the calculated Q_s from the theoretical Q_s values, where the theoretically determined Q_s of 6.53 kWh presented 100% of the energy and the calculated Q_s the corresponding percentage. The results are presented in Table 4. As visible from the table, the deviation increases with the inlet

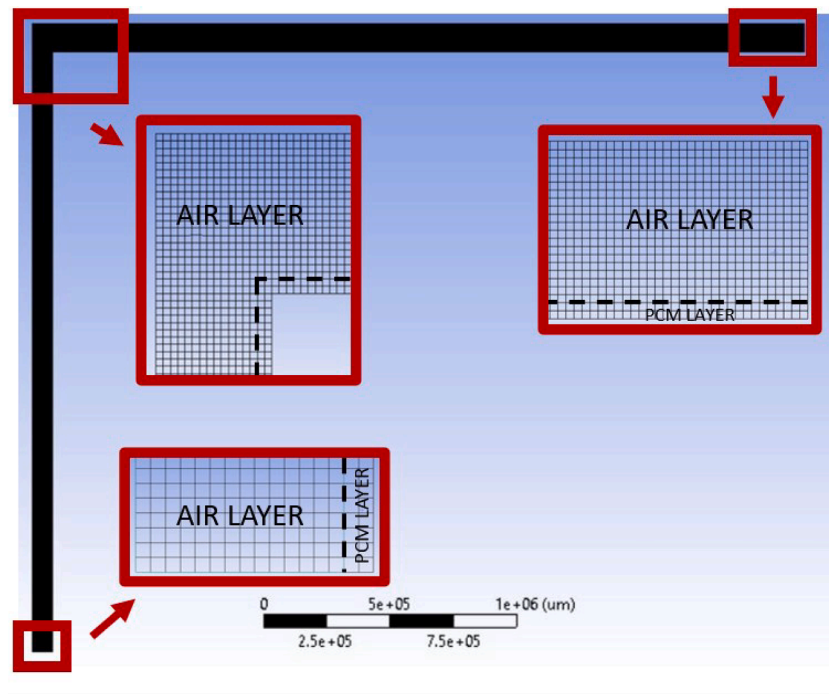


Fig. 20. The selected grid with element size of 5 mm.

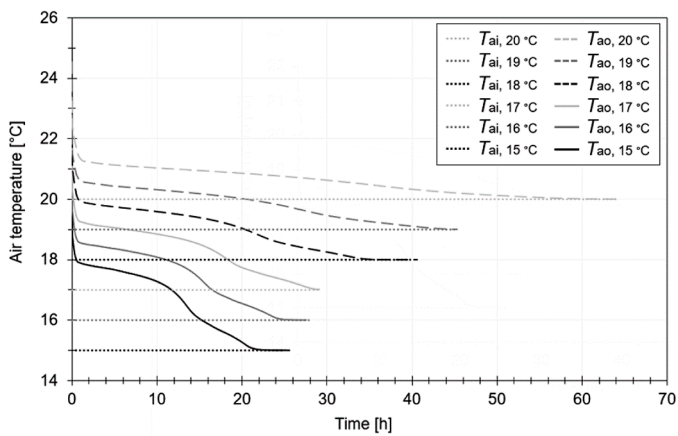


Fig. 21. Outlet air temperatures obtained in adiabatic conditions for different inlet air temperature scenarios.

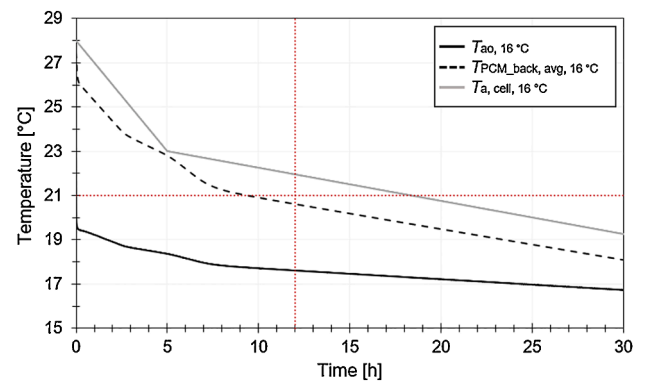


Fig. 23. The results obtained at inlet air temperature of 16 °C.

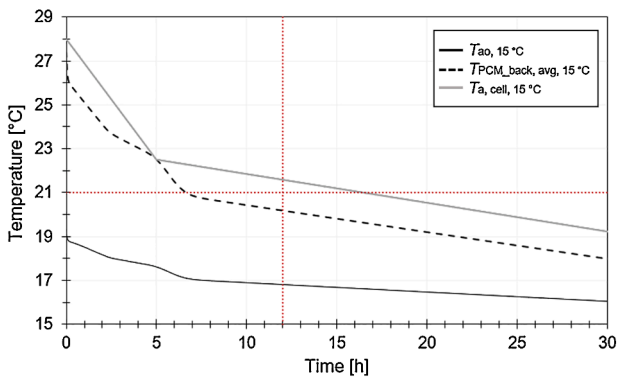


Fig. 22. The results obtained at inlet air temperature of 15 °C.

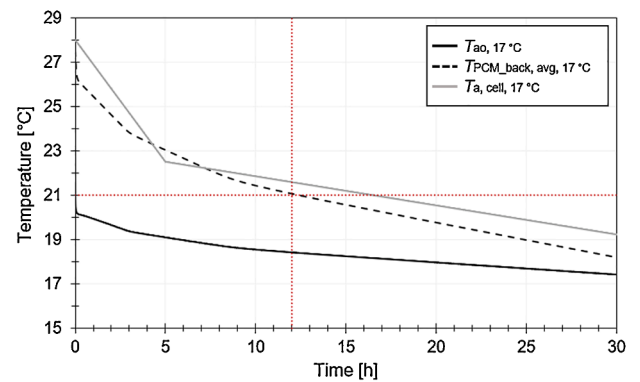


Fig. 24. The results obtained at air inlet temperature of 17 °C.

Table 4
Calculated energy released from the plates Q_s and the deviation from the theoretical value of Q_s .

Inlet temperature	15 °C	16 °C	17 °C	18 °C	19 °C	20 °C
Energy released Q_s [kWh]	6.34	6.28	6.22	6.16	6.04	5.93
Deviation from theoretical value* [%]	3.0	3.8	4.8	5.7	7.5	9.2

* 6.53 kWh (in the temperature range: 14–30 °C).

air temperature, as higher inlet temperatures cannot release the energy stored at lower temperatures of the PCM material.

3.4. Determination of energy use of APS operation

As shown in Fig. 25 the proposed APS underperforms in comparison to class A+++ and class G air conditioner from energy use point of view. To produce 6.34 kWh of cooling energy the APS consumes 4.6 kWh, class G air conditioner 3.3 kWh and class A+++ air conditioner 1.2 kWh.

Furthermore, Fig. 26 shows the cost of consumed electrical energy to produce 6.34 kWh of cooling energy for class A+++ and class G air conditioner, as well as for APS proposed in this study. The prices of electrical energy were taken after ('Documents & price lists for energy electricity by Elektro energija', 2022) and are 0.13999 eur/kWh (day rate) and 0.09999 eur/kWh (night rate). Both, class A+++ and G air conditioners operate in day rate, therefore, the operation cost would be approximately 0.174 eur/day (class A+++) and 0.467 eur/day (class G), respectively. On the other hand, APS operates in night rate, therefore, the operation cost would be 0.462 eur/day.

4. Discussion

4.1. Simulated results

Complete solidification of PCM during the nighttime cycle is crucial for efficient performance and sufficient cooling effect of PCM during the day when its application is required to cool the indoor spaces. Fig. 27 shows the outlet temperatures obtained during each of the inlet temperature scenarios. Due to the influence of the high airflow rates, inlet air velocities, and the boundary condition of cell air temperatures, the outlet air temperatures do not show a clear phase change curve. Therefore, they cannot serve as an indicator of solidification time. However, it is clear that inlet temperatures affect outlet temperatures. In Figures Figs. 27,28, the horizontal and vertical red dotted lines represent the temperature limit of 21 °C and the end of the nighttime cycle at 12 h, respectively.

Compared to the outlet air temperatures (T_{ao}), the average surface temperature on the back of the PCM plates ($T_{PCM_back, avg}$) clearly shows

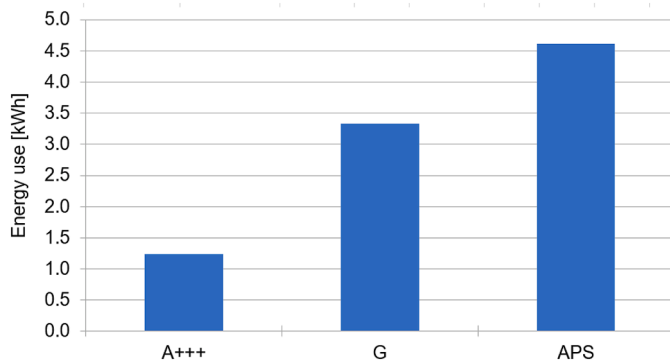


Fig. 25. Electrical energy use to produce 6.34 kWh of cooling energy of the best case (A+++ class) and the worst case (G class) air conditioner in comparison to the proposed APS.

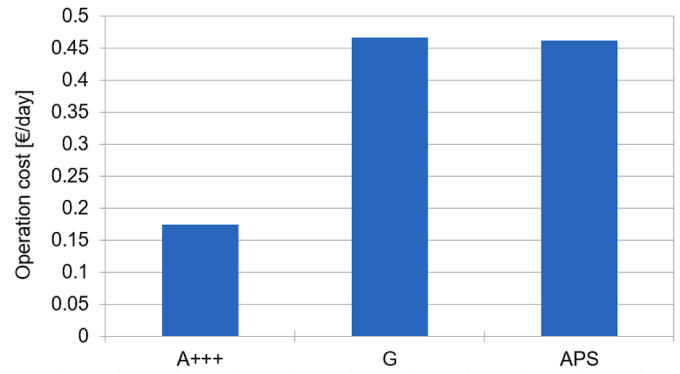


Fig. 26. The cost of consumed electrical energy per day of operation to produce 6.34 kWh of cooling energy of the best case (A+++ class) and the worst case (G class) air conditioner in comparison to the proposed APS.

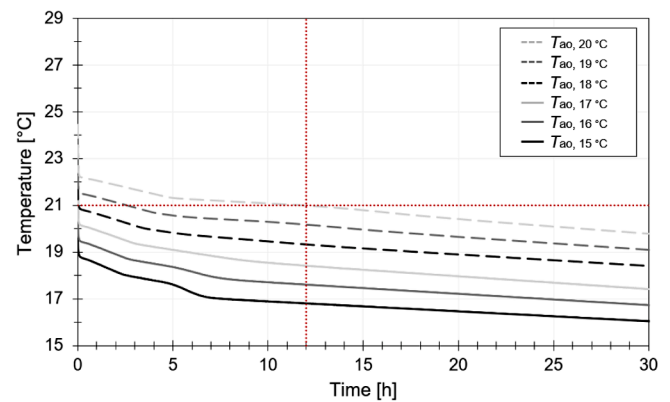


Fig. 27. The area-weighted average outlet air temperatures simulated within corresponding inlet temperature scenario.

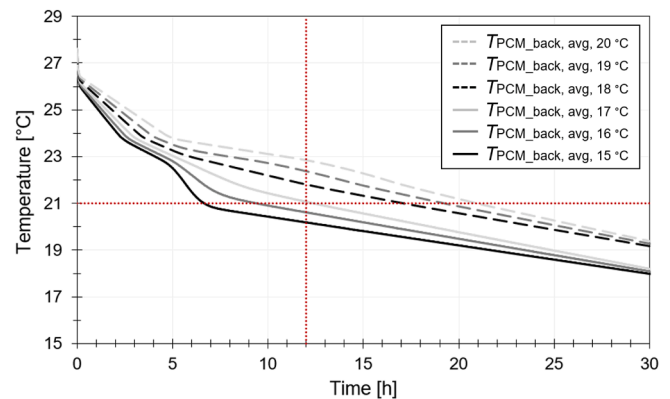


Fig. 28. The area-weighted average back surface PCM temperatures simulated within corresponding scenario.

the completed solidification time (Fig. 28). The figure shows that solidification is completed in 7 h when the inlet air has a temperature of 15 °C. The optimum time for solidification is reached after 9 h when the inlet air has a temperature of 16 °C. The results show that, the PCM can be solidified during the night cycle after 12 h even when the air is injected into the air gap at 17 °C. The insufficient solidification time was achieved under conditions where the temperature difference between PCM and the inlet temperature is too small. For example, at inlet temperatures of 18 °C, 19 °C and 20 °C, 17 h, 19 h and 21 h, respectively, were required to complete PCM solidification. Based on this study,

where only the effect of one PCM was studied it is difficult to draw any other conclusions which would base on different PCM solidification temperature points.

However, the solidification time could be drastically improved if the PCM was cooled from two sides - room side and the air gap side. This could be accomplished by opening the windows during the night or ventilating the room with the cool, unconditioned outdoor air. While opening the windows requires additional manual maintenance, mechanical operation of room ventilation systems requires additional energy input. The combination of these possible air-based PCM cooling methods (mechanically ventilated air gap, opening the windows, and mechanical ventilation) could present the optimal solution for the reference case of microclimate in a building in terms of energy use.

4.2. Comparison of results from present study to other investigations

The results obtained in this study can be compared with some other relevant studies.

4.2.1. Thermal performance

For example, Diarce et al. studied a 2D model in ANSYS Fluent of macroencapsulated PCM (RT35; $T_m = 35\text{ }^\circ\text{C}$) positioned in hollow aluminium profiles of the external layer (thickness 2 cm) for a seasonal application (Diarce et al., 2014). Heat transfer from the air gap to the PCM in the wall was enhanced by the short horizontal aluminium fins inclined toward the air gap. On the inner side of the 6 cm wide air gap, which was ventilated with an additional fan, there was an XPS insulation layer. To simulate the heat transfer in the air gap, a DO (Discrete Ordinates) radiation model was applied in the air gap between the PCM aluminium wall and the XPS layer, which improved the accuracy of the temperatures on the XPS wall according to the experimentally measured temperatures (without using the radiation model, the temperature difference of the XPS surface reached $2.6\text{ }^\circ\text{C}$). The airflow rate studied ranged from $97.2\text{ m}^3/\text{h}$ to $277.2\text{ m}^3/\text{h}$ with inlet temperatures between $0\text{ }^\circ\text{C}$ and $10\text{ }^\circ\text{C}$ and velocities up to 0.93 m/s .

Furthermore, Hu and Heiselberg used COMSOL Multiphysics to calculate a 2D model of a 10 cm wide heat exchanger with PCM plates ($T_m = 22\text{ }^\circ\text{C}$) for summer cooling in Copenhagen, Denmark, placed in the glazed exterior wall with 60 PCM plates (5–20 mm thick, 10 mm thick is optimal in terms of cooling effect) separated by air gaps (5 mm wide) (Hu & Heiselberg, 2018). The tested velocities in the air gaps were between $0.74\text{--}1.78\text{ m/s}$ and $00:00\text{--}4:00$ (4 h) at an air inlet temperature of $14\text{ }^\circ\text{C}$. The nighttime was shorter compared to the other studies because the system was tested in colder climates and therefore, the plates could consolidate sufficiently within the night cycle.

In addition, Kant et al. studied a PCM layer (4 cm; $T_m = 26.6\text{ }^\circ\text{C}$; $28.2\text{ }^\circ\text{C}$ and $32\text{ }^\circ\text{C}$) applied on the BiPV wall and separated from the concrete wall by an air gap (8 cm) and calculated it using the COMSOL Multiphysics 5.0 software tool (Kant et al., 2019). The nightly cycle lasted 10 h at an inlet temperature of $25\text{ }^\circ\text{C}$, as the PV system is pre-heated to temperatures of $60\text{ }^\circ\text{C}$ or higher. Similar to Diarce et al. the model was simulated using the radiation model (Diarce et al., 2014). The PCM was also modelled using the solidification and melting model.

Similarly, Li et al. created a 2D model of a double-skin glazing façade (air gap width of 45 cm) with laminated composite blinds PCM (PX35; $T_m = 35\text{ }^\circ\text{C}$; 15 cm wide and 0.3 cm thick) using the ANSYS Fluent software tool (Li et al., 2019). The model was calculated using the k- ϵ viscosity model and the DO radiation model. The inlet air temperatures varied between $25\text{ }^\circ\text{C}$ and $27\text{ }^\circ\text{C}$ at supply air velocities of 0.45 m/s . The ambient temperature varied between 26 and $40\text{ }^\circ\text{C}$. The surface temperature of the inner façade was reduced to about $2.9\text{ }^\circ\text{C}$ (compared to the surface temperature of the external façade). The peak surface temperatures of the PCM layer reached at noon (12:00) were between $38\text{ }^\circ\text{C}$ and $40\text{ }^\circ\text{C}$, and the temperature difference between inlet and outlet air varied between $3\text{ }^\circ\text{C}$ and $3.5\text{ }^\circ\text{C}$. Within the cases investigated within the present study, on average, the temperature difference reached $2\text{ }^\circ\text{C}$ in all

studied inlet temperature scenarios.

The previous cases of air gap walls in contact with PCM layers were tested as 2D models. In contrast, Faheem et al. tested the PCM for cooling (microencapsulated PCM, $T_m = 19\text{ }^\circ\text{C}$ and $20\text{ }^\circ\text{C}$) in low thermal mass buildings with a 3D model in ANSYS Fluent 14 (Faheem et al., 2016). The inlet air temperature of $12\text{ }^\circ\text{C}$ was lower compared to previous studies, and the PCM T_m are also lower. Nighttime ventilation was in operation between 18:00 and 6:00 (12 h). The effects of velocities were significant at PCM ($T_m = 20\text{ }^\circ\text{C}$) and were less than 2 m/s , and at PCM ($T_m = 19\text{ }^\circ\text{C}$) they reached 5 m/s . During the nighttime cycle at 0:00, average surface temperatures at the bottom of the slab dropped by $1.5\text{ }^\circ\text{C}$, while room air temperatures dropped by $4\text{ }^\circ\text{C}$. In the present study, the model predicts that indoor cell temperatures drop by about $4\text{ }^\circ\text{C}$ during the first 5 h and in the last 15 h by $2.2\text{ }^\circ\text{C}$.

Similarly, Yu et al. used ANSYS Fluent to calculate a 3D model of the shape-stabilised outer layer PCM of the ventilated roof (different summers $T_m = 34\text{--}38\text{ }^\circ\text{C}$ and thicknesses between $2.5\text{--}3.5\text{ cm}$) (Yu et al., 2020). The best results were obtained with inlet air velocities between $1.9\text{--}2.5\text{ m/s}$ and inlet temperatures of $24\text{--}25\text{ }^\circ\text{C}$. In two cases studied during the hot summer, the ventilation was conducted from 18:00 h for 13–15 h and from 19:00 h for 11–12 h to fully consolidate the PCM layer.

A concept very similar to the one proposed in this study was presented by Evola et al. using Energy Plus software to study a ventilated internal PCM (Micronal T23® - 60% microencapsulated; peak $T_m = 26.7\text{ }^\circ\text{C}$ and 2 cm thick) with a 3 cm air gap (Evola et al., 2014). The air gap was ventilated with an airflow of $168\text{ m}^3/\text{h}$ and a velocity of 0.65 m/s between 21:00–6:00 h (9 h) at an air inlet temperature of $20\text{ }^\circ\text{C}$, a wall surface temperature of $27\text{ }^\circ\text{C}$, and an air outlet temperature of $24.5\text{ }^\circ\text{C}$. In the present study, the temperature difference between inlet and outlet air temperatures was smaller ($2\text{ }^\circ\text{C}$) compared to the study by Evola et al. where the temperature difference reached up to $4.5\text{ }^\circ\text{C}$.

In addition, Weinsläder et al. experimentally tested a ventilated chilled ceiling with PCM in a suspended ceiling (PCM DELTA®- COOL 24, $T_m = 24\text{ }^\circ\text{C}$) (Weinsläder et al., 2014). With an airflow of $300\text{ m}^3/\text{h}$ (the highest tested reached $600\text{ m}^3/\text{h}$) supplied between 21:00–5:00 (8 h) at an air inlet temperature of $16\text{ }^\circ\text{C}$, the surface temperatures measured on the back side of the PCM panels dropped below $24\text{ }^\circ\text{C}$ after 8 h of the experiment. The solidification time presented in the study by Weinsläder et al. is comparable to the results of the present study, where the plates solidified in 7 h at an air inlet temperature of $15\text{ }^\circ\text{C}$.

The values tested in the present study are within the range of the other studies discussed. In fact, the studies have shown that the temperature differences tested between the inlet air temperatures and the melting temperatures of PCM range from $7\text{ }^\circ\text{C}$ to $14\text{ }^\circ\text{C}$ ($7\text{--}9\text{ }^\circ\text{C}$ in the present study), so that the plates could solidify overnight. The airflow rates studied mostly varied between $97.2\text{ m}^3/\text{h}$ and $600\text{ m}^3/\text{h}$ (present study: $450\text{ m}^3/\text{h}$) with air gap velocities between 0.45 m/s and 5 m/s (present study: 0.8 m/s). The duration of the night cycle varied between 4 h and 15 h, but averaged between 8 h and 12 h (present study: 12 h; 7–12 h for complete solidifications). The temperature differences between the inlet and outlet air temperatures are smaller in the present study compared to the other studies, but still reasonable. Thus, the solidification time depends on the temperature difference between the inlet air temperatures and the PCM melting temperatures, the amount and heat storage capacity of the PCM, the type of encapsulation, and the characteristics of the airflow in the air gap (airflow rate and velocity).

4.2.2. Energy performance

Due to different methods of energy performance determination among the reviewed studies, the comparison of the results of the present study to them is limited. Moreover, many studies do not present the results of systems' energy performance, but only the temperature distribution (Faheem et al., 2016; Yu et al., 2020; Diarce et al., 2014; Li et al., 2019). The energy performance of the systems was determined only, when PCM plates were not in the direct contact with the indoor space (room) because the heat flux could be monitored.

For example, Evola et al. used Energy Plus for the determination of daily energy use for cooling and concluded that the presence of ventilated air gap decreased the energy from 185.0 Wh/(m².day) to 107.3 Wh/(m².day) (Evola et al., 2014). In present study the cooling effect of the plates to the room could not be assessed directly and therefore, neither the presence of the ventilated air gap. However, considering the floor area of the room to be 7.32 m² and the total theoretical cooling capacity of the plates 6.53 kWh, the cooling effect of the plates may contribute to 892.1 Wh/(m².day). The cooling capacity of the APS system in the present study is much larger than in the referenced one, since the value is theoretical and not based on the calculated room temperatures and the amount of PCM mass in this study is much larger (reference study: microencapsulated plates).

Furthermore, Hu and Heiselberg closed PCM into a ventilated wall (heat exchanger) and ventilated it over the day and over the night. Over the night, the 10 mm thick PCM discharged 3.55 MJ (0.981 kWh) and over the day charged 3.19 MJ (0.886 kWh) of heat (Hu & Heiselberg, 2018). The setup of the reference study has a different purpose compared to the present (the room is cooled by the outlet air and not by the PCM plates in contact of the room air directly) which results in the lower amount of energy needed for cooling. Also, the system is dimensioned for a cooler climate type with lower cooling demand. Nevertheless, as the study investigated a closed system of heat exchanger, the room wall boundary conditions didn't play a crucial role in the determination of PCM solidification which could be determined only based on the outlet temperatures. Similar conclusion based on the experimental setup is aligned with the experimental investigation by Osterman et al. where an active ventilated PCM heat storage for ventilation system was investigated with 30 PCM plates (1.361 kg of RT22HC with heat storage capacity of 181 kJ/kg per plate;) mounted into a rectangular EPS box. When the plates were preheated to 25 °C and ventilated with T_{ai} of 16 °C they released 5.1 MJ (1.42 kWh) of energy (Osterman et al., 2015).

Weinläder et al. presented a case of ventilated PCM ceiling (Weinläder et al., 2014) and determined the total cooling power of the system by summing the cooling power of the air in the ventilated ceiling (based on the temperature difference between the inlet and outlet temperature measured in the air gap) and cooling power of the PCM through the plaster board ceiling (based on the temperature difference of temperatures measured on the front and on the back of the gypsum plate). They found that in the conference room, the total cooling power yields 7.50 kWh (theoretical 7.92 kWh) which is close to the total storage capacity of the PCM plates. Compared to APS system (the present study), the total storage capacity of the PCM plates is 6.53 kWh and similar to the compared case. However, in this case the total cooling power of the system cannot be calculated because the PCM plates are in direct contact with the air and the temperature difference on the front and on the back of the gypsum plate cannot be determined. In the comparing study, during the nighttime solidification cycle (duration: 8 h) the ventilation flow rates of 300 m³/s and 600 m³/s were established at fans operating power of 60 W and 150 W, respectively and consumed 1.68 kWh of electrical energy which is higher than the electrical energy consumed in the present study (0.57 kWh).

Navarro et al. experimentally investigated ventilated concrete slab filled with PCM modules (tubes) (Navarro et al., 2016). The system's operation (fan and heat pump together) consumed between 4 kWh/day and 1.2 kWh/day. Compared to this study, the fan operation present between 0.57 kWh/day (solidification time of 7 h and T_{ai} of 15 °C) and 0.98 kWh/day (solidification time of 12 h and T_{ai} of 17 °C) depending on the solidification time and inlet temperature.

Prabhakar et al., simulated and optimized the model of single-family house with PCM plates (optimised $T_m = 22-26$ °C depending on the location) in CSM cases integrated in the internal building elements (interior walls, internal partition walls and ceiling) without the presence of air gap with EnergyPlus and GenOpt v3.1.1 (Prabhakar et al., 2020). By using PCM, the maximum energy savings were determined in

Ceduna, South Australia of 26.31%. In the temperate climate conditions, by coupling a PCM passive system with night ventilation, the effectiveness of PCM was increased from 3.32% to 25.62% and was even more improved (to 40%) when coupled with temperature-controlled ventilation. Within this study, the energy savings cannot be determined and compared, since our outdoor boundary conditions are limited to only one day scenario and nighttime solidification cycle. However, the results of this study stress the importance of the correctly applied ventilation on the effectiveness of PCM performance.

Similarly to the present study where the PCM plates were installed on the internal wall in contact with the room air, Gracia et al. experimentally tested a ventilated external walls with PCM plates located in its air gap (De Gracia et al., 2013). In the experimental conditions in July and August the heat stored and released by the PCM was investigated. During the night, the PCM system stored 20.25 MJ (5.62 kWh) and 25.90 MJ (7.19 kWh) in July and August season, respectively. During the day, the PCM system released 2.20 MJ (0.61 kWh) and 0.10 MJ (0.03 kWh) in July and August season, respectively. Comparing the results from the present study to the reference, the released energy is comparable to the theoretical energy storage capacity of the plates.

Comparing energy performance of the APS system to air-conditioning (AC) devices with energy classes A+++ and G shows that the APS system consumes more energy compared to both AC devices. When comparing the three systems based on the operational costs the performance of APS improves. AC devices cool during the daily cycles with higher electricity prices, while the APS system uses electricity over the night when the electricity tariffs are lower. It is shown that the operation costs of A+++ class AC device are lower compared to the APS system and that G class AC device has the highest costs. Therefore, based on the operation costs it is cheaper to renovate the building with APS system than inefficient AC device. However, the construction costs of the APS might be higher than of the AC device since the APS system is still a technology under the development. Nevertheless, despite the fact that the energy consumption of the APS is higher compared to the AC-devices, the calculated results reveal that the APS system has a recognisable potential for cooling application, especially considering the fact that AC devices are already a developed and optimized technology meanwhile the current APS configuration is still in its first prototype form.

It should be noted that simulating a parametric case of the proposed system in ANSYS Fluent is a challenging task due to an unknown boundary condition that significantly affects the results. Such an objective would be more likely to be achieved by using Energy Plus or TRNSYS software. However, these do not provide results with detailed temperature distribution along the studied model.

5. Conclusions

The present study investigates the performance of the proposed passive-active PCM system for cooling application during the free cooling nighttime cycle, where the PCM is solidified under the different inlet temperature scenarios representative of southern and central European climates (Mediterranean climate).

The results show the solidification time of PCM with a melting temperature of 24 °C when cooled with inlet temperatures of 15 °C, 16 °C, 17 °C, 18 °C, 19 °C, and 20 °C.

- The model has some uncertainty in the room air temperature conditions during the solidification times but shows realistic solidification times based on the measured results.
- The study showed that solidification was completed within the nighttime cycle at inlet temperatures of 15 °C, 16 °C and 17 °C, making the inlet temperatures optimal among the cases studied.
- The solidification time of the PCM can be improved by increasing the airflow rates in the air gap or by combining the nighttime ventilation in the air gap simultaneously with the ventilation from the room side

(natural - window opening or mechanical ventilation), so that the PCM plates are cooled from both sides. In this way, the plates could be solidified in time even at higher than recommended outdoor air temperatures (18 °C, 19 °C and 20 °C). Also, the performance of the system may be improved with the addition of metal structures either mixed into the PCM material or added as structural elements connecting PCM plates to the air gap (metal fins) for improved heat conductivity from the air to the PCM.

- At this point, the results on energy performance and operating costs of the APS system under the static conditions investigated in the framework of this study show, that APS system has higher energy use and operational costs than A+++ class air-conditioning device (73% and 62%, respectively). The APS has higher energy use and lower operation cost than G class air-conditioning device (27% and 1%, respectively).
- The amount of cooling energy 6.34 kWh corresponds to the amount of PCM available in PCM for cooling. Based on the results from the experimental study, it can be concluded, that the sufficiency of the cooling energy amount depends on the thermal conditions and air velocities in the room, because the system doesn't operate actively during the day. This means that the PCM plates have a certain cooling power, which is higher when the outdoor air temperatures and indoor air velocities are high. However, the duration of cooling effect is shorter compared to combination of lower temperatures and air velocities. With the results, it has been shown, that during the required period of time, such amount of cooling energy in PCM would be sufficient to adequately decrease the indoor temperatures. Although further tests would be required to optimise the system accordingly.
- Nevertheless, this is the amount of cooling energy available in PCM of APS under the current configuration and therefore, the AC systems are evaluated on the same basis – regardless of whether they would reach the required thermal comfort or not. Since this is the limitation of this model, this research should be extended with another study holistically evaluating the performance of such systems during the daytime cycle.

Declaration of Competing Interest

The authors declare that they have no known competing financial interests or personal relationships that could have appeared to influence the work reported in this paper.

Data availability

Data will be made available on request.

Acknowledgement

The authors acknowledge the financial support from the Slovenian Research Agency (research core funding No. P2-0223, Heat and Mass Transfer, No. P2-0158, Structural engineering and building physics; No. P2-0422, Functionalised fluids for advanced energy systems). This study was financially supported by the Région Auvergne-Rhône-Alpes.

References

- T. Abergel and C. Delmastro, 'Is cooling the future of heating? – Analysis - IEA', 2020. <https://www.iea.org/commentaries/is-cooling-the-future-of-heating> (Accessed November 20, 2021).
- Statistical office of the European Union EUROSTAT, 'Energy consumption in households', 2020.
- 'The Future of Cooling – Analysis - IEA'. <https://www.iea.org/reports/the-future-of-cooling> (Accessed December 23, 2019).
- C. Delmastro, T. Abergel, K. Lane, and Y. Monschauer, 'Cooling – analysis - IEA', 2021. <https://www.iea.org/reports/cooling> (Accessed November 20, 2021).

- Isaac, M., & van Vuuren, D. P. (2009). Modeling global residential sector energy demand for heating and air conditioning in the context of climate change. *Energy Policy*. <https://doi.org/10.1016/j.enpol.2008.09.051>
- Liu, C., Kershaw, T., Fosas, D., Ramallo Gonzalez, A. P., Natarajan, S., & Coley, D. A. (2017). High resolution mapping of overheating and mortality risk. *Building and Environment*, 122, 1–14. <https://doi.org/10.1016/j.buildenv.2017.05.028>
- Lomas, K. J., & Porritt, S. M. (2017). Overheating in buildings: Lessons from research. *Building Research and Information*, 45(1–2), 1–18. <https://doi.org/10.1080/09613218.2017.1256136>
- Bundle, N., O'Connell, E., O'Connor, N., & Bone, A. (2018). A public health needs assessment for domestic indoor overheating. *Public Health*, 9–15. <https://doi.org/10.1016/j.puhe.2017.12.016>
- Al-Yasiri, Q., & Szabó, M. (2023). Numerical analysis of thin building envelope-integrated phase change material towards energy-efficient buildings in severe hot location. *Sustainable Cities and Society*, 89, Article 104365. <https://doi.org/10.1016/j.scs.2022.104365>
- Arkar, C., Domjan, S., & Medved, S. (2018). Lightweight composite timber façade wall with improved thermal response. *Sustainable Cities and Society*, 38, 325–332. <https://doi.org/10.1016/j.scs.2018.01.011>
- De Masi, R. F., Gigante, A., & Vanoli, G. P. (2020). Numerical analysis of phase change materials for optimizing the energy balance of a nearly zero energy building. *Sustainable Cities and Society*, 63, Article 102441. <https://doi.org/10.1016/j.scs.2020.102441>
- Fateh, A., Borelli, D., Weindlader, H., & Devia, F. (2019). Cardinal orientation and melting temperature effects for PCM-enhanced light-walls in different climates. *Sustainable Cities and Society*, 51, Article 101766. <https://doi.org/10.1016/j.scs.2019.101766>
- Duraković, B., & Mešetović, S. (2019). Thermal performances of glazed energy storage systems with various storage materials: An experimental study. *Sustainable Cities and Society*, 45, 422–430. <https://doi.org/10.1016/j.scs.2018.12.003>
- Li, S., Sun, G., Zou, K., & Zhang, X. (2016). Experimental research on the dynamic thermal performance of a novel triple-pane building window filled with PCM. *Sustainable Cities and Society*, 27, 15–22. <https://doi.org/10.1016/j.scs.2016.08.014>
- Li, S., Zou, K., Sun, G., & Zhang, X. (2018). Simulation research on the dynamic thermal performance of a novel triple-glazed window filled with PCM. *Sustainable Cities and Society*, 40, 266–273. <https://doi.org/10.1016/j.scs.2018.01.020>
- Zavrli, E., Zupan, G., Stritih, U., & Dovjak, M. (2020). Overheating reduction in lightweight framed buildings with application of phase change materials. *Strojinski Vestnik - Journal of Mechanical Engineering*, 66, 3–14. <https://doi.org/10.5545/sv-jme.2019.6244>
- Ostry, M., & Becovsky, D. (2009). Influence of panels with phase change materials on the thermal stability of attic spaces. In *8th IIR conference on phase change materials and slurries for refrigeration and air conditioning, Karlsruhe*.
- Prabhakar, M., Saffari, M., de Gracia, A., & Cabeza, L. F. (2020). Improving the energy efficiency of passive PCM system using controlled natural ventilation. *Energy and Buildings*, 228, Article 110483. <https://doi.org/10.1016/j.enbuild.2020.110483>
- Agarwal, P., & Prabhakar, A. (2023). Energy and thermo-economic analysis of PCM integrated brick in composite climatic condition of Jaipur - A numerical study. *Sustainable Cities and Society*, 88, Article 104294. <https://doi.org/10.1016/j.scs.2022.104294>
- Ahangari, M., & Maerefat, M. (2019). An innovative PCM system for thermal comfort improvement and energy demand reduction in building under different climate conditions. *Sustainable Cities and Society*, 44, 120–129. <https://doi.org/10.1016/j.scs.2018.09.008>
- Belmonte, J. F., Eguía, P., Molina, A. E., & A, J. (2015). Almendros-Ibáñez, 'Thermal simulation and system optimization of a chilled ceiling coupled with a floor containing a phase change material (PCM)'. *Sustainable Cities and Society*, 14, 154–170. <https://doi.org/10.1016/j.scs.2014.09.004>
- Rathore, P. K. S., Gupta, N. K., Yadav, D., Shukla, S. K., & Kaul, S. (2022). Thermal performance of the building envelope integrated with phase change material for thermal energy storage: An updated review. *Sustainable Cities and Society*, 79, Article 103690. <https://doi.org/10.1016/j.scs.2022.103690>
- Osterman, E., Hagel, K., Rathgeber, C., Butala, V., & Stritih, U. (2015). Parametrical analysis of latent heat and cold storage for heating and cooling of rooms. *Applied Thermal Engineering*, 84, 138–149. <https://doi.org/10.1016/j.applthermaleng.2015.02.081>
- Abdo, P., Huynh, B. P., Braytee, A., & Taghipour, R. (2020). An experimental investigation of the thermal effect due to discharging of phase change material in a room fitted with a windcatcher. *Sustainable Cities and Society*, 61, Article 102277. <https://doi.org/10.1016/j.scs.2020.102277>
- Hou, M., Kong, X., Li, H., Yang, H., & Chen, W. (2021). Experimental study on the thermal performance of composite phase change ventilated roof. *Journal of Energy Storage*, 33, Article 102060. <https://doi.org/10.1016/j.est.2020.102060>
- Lizana, J., de-Borja-Torrejon, M., Barrios-Padura, A., Auer, T., & Chacartegui, R. (2019). Passive cooling through phase change materials in buildings. A critical study of implementation alternatives. *Applied Energy*, 254, Article 113658. <https://doi.org/10.1016/j.apenergy.2019.113658>
- Weindlader, H., Körner, W., & Strieder, B. (2014). A ventilated cooling ceiling with integrated latent heat storage - Monitoring results. *Energy and buildings*, 82, 65–72. <https://doi.org/10.1016/j.enbuild.2014.07.013>
- Jiao, F., & Xu, P. (2015). Simulation and feasibility analysis of PCM based passive cooling technique in residential house. *Procedia engineering* (pp. 1969–1976). Elsevier Ltd. <https://doi.org/10.1016/j.proeng.2015.09.189>
- Faheem, A., Ranzì, G., Fiorito, F., & Lei, C. (2016). A numerical study on the thermal performance of night ventilated hollow core slabs cast with micro-encapsulated PCM concrete. *Energy and Buildings*, 127, 892–906. <https://doi.org/10.1016/j.enbuild.2016.06.014>

- Yu, J., et al. (2020). Study on thermal insulation characteristics and optimized design of pipe-embedded ventilation roof with outer-layer shape-stabilized PCM in different climate zones. *Renewable Energy*, 147, 1609–1622. <https://doi.org/10.1016/j.renene.2019.09.115>
- Morovat, N., Athienitis, A. K., Candanedo, J. A., & Dermalidros, V. (2019). Simulation and performance analysis of an active PCM-heat exchanger intended for building operation optimization. *Energy and buildings*, 199, 47–61. <https://doi.org/10.1016/j.enbuild.2019.06.022>
- Navarro, L., de Gracia, A., Castell, A., & Cabeza, L. F. (2016). Experimental study of an active slab with PCM coupled to a solar air collector for heating purposes. *Energy and Buildings*, 128, 12–21. <https://doi.org/10.1016/j.enbuild.2016.06.069>
- Evola, G., Marletta, L., & Sicurella, F. (2014). Simulation of a ventilated cavity to enhance the effectiveness of PCM wallboards for summer thermal comfort in buildings. *Energy and Buildings*, 70, 480–489. <https://doi.org/10.1016/j.enbuild.2013.11.089>
- De Gracia, A., Navarro, L., Castell, A., Ruiz-Pardo, Á., Álvarez, S., & Cabeza, L. F. (2013). Thermal analysis of a ventilated facade with PCM for cooling applications. *Energy and Buildings*, 65, 508–515. <https://doi.org/10.1016/j.enbuild.2013.06.032>
- Diarce, G., et al. (2013). Ventilated active façades with PCM. *Applied Energy*, 109, 530–537. <https://doi.org/10.1016/j.apenergy.2013.01.032>
- Diarce, G., Campos-Celador, Á., Martín, K., Urresti, A., García-Romero, A., & Sala, J. M. (2014). A comparative study of the CFD modeling of a ventilated active façade including phase change materials. *Applied Energy*, 126, 307–317. <https://doi.org/10.1016/j.apenergy.2014.03.080>
- Zhou, Y., Yu, C. W. F., & Zhang, G. (2018). Study on heat-transfer mechanism of wallboards containing active phase change material and parameter optimization with ventilation. *Applied Thermal Engineering*, 144, 1091–1108. <https://doi.org/10.1016/j.applthermaleng.2018.04.083>
- Hu, Y., & Heiselberg, P. K. (2018). A new ventilated window with PCM heat exchanger—Performance analysis and design optimization. *Energy and Buildings*, 169, 185–194. <https://doi.org/10.1016/j.enbuild.2018.03.060>
- Kant, K., Pitchumani, R., Shukla, A., & Sharma, A. (2019). Analysis and design of air ventilated building integrated photovoltaic (BIPV) system incorporating phase change materials. *Energy Conversation and Management*, 196, 149–164. <https://doi.org/10.1016/j.enconman.2019.05.073>
- Li, Y., Darkwa, J., Kokogiannakis, G., & Su, W. (2019). Phase change material blind system for double skin façade integration: System development and thermal performance evaluation. *Applied Energy*, 252, Article 113376. <https://doi.org/10.1016/j.apenergy.2019.113376>
- Zavr1, E., El Mankibi, M., Dovjak, M., & Stritih, U. (2022a). Enhancing performance of building elements with phase change materials for cooling with air-based systems. *Journal of Energy Storage*, 51, Article 104461. <https://doi.org/10.1016/j.est.2022.104461>
- Han, Y., & Taylor, J. E. (2016). Simulating the Inter-Building Effect on energy consumption from embedding phase change materials in building envelopes. *Sustainable Cities and Society*, 27, 287–295. <https://doi.org/10.1016/j.scs.2016.03.001>
- Mourid, A., El Alami, M., & Kuznik, F. (2018). Experimental investigation on thermal behavior and reduction of energy consumption in a real scale building by using phase change materials on its envelope. *Sustainable Cities and Society*, 41, 35–43. <https://doi.org/10.1016/j.scs.2018.04.031>
- Blumenfeld, A., Thumm, W. T., & Phelps, H. (2014). Passive building systems vs. active building systems and the return on investment. *Building Innovation Conference and Expo*.
- Zavr1, E., El Mankibi, M., Dovjak, M., & Stritih, U. (2022b). Experimental investigation of air-based active-passive system for cooling application in buildings. *Sustainable Cities and Society*, 85, Article 104031. <https://doi.org/10.1016/j.scs.2022.104031>
- White, F. M. (1998). *Fluid mechanics* (4th ed.). McGraw-Hill College.
- Raj, V. A. A., & Velraj, R. (2011). Heat transfer and pressure drop studies on a PCM-heat exchanger module for free cooling applications. *International Journal of Thermal Sciences*, 50(8), 1573–1582. <https://doi.org/10.1016/j.ijthermalsci.2011.01.025>
- Munson, B. R., Rothmayer, A. P., Okiishi, T. H., & Huebsch, W. W. (2012). *Fundamentals of fluid mechanics* (7th ed.). Wiley.
- Rostamizadeh, M., Khanlarkhani, M., & Sadrameli, S. M. (2012). Simulation of energy storage system with phase change material (PCM). *Energy and Buildings*, 49, 419–422. <https://doi.org/10.1016/j.enbuild.2012.02.037>
- Osterman, E. (2015). Doktorska naloga: Sistem z latentnim hranilnikom toplote za ogrevanje in hlajenje prostorov. *Fakulteta za strojništvo*. Univerza v Ljubljani. 'Rubitherm GmbH'. <https://www.rubitherm.eu/en/productCategories.html> (Accessed November 21, 2021).
- Rubitherm, 'Data Sheet Rubitherm SP24E', 2020. https://www.rubitherm.eu/media/products/datasheets/Techdata_-SP24E_EN_09112020.PDF (Accessed November 24, 2021).
- EN 15251:2007:E, 'Indoor environmental input parameters for design and assessment of energy performance of buildings addressing indoor air quality, thermal environment, lighting and acoustics', 2007.
- Ruiz, G. R., & Bandera, C. F. (2017). Validation of calibrated energy models: Common errors. *Energies*, 10(10). <https://doi.org/10.3390/en10101587>
- 'Fluent 13.0 Lecture06-Turbulence Near Wall | PDF | Reynolds Number | Turbulence', *Scribd*. <https://www.scribd.com/document/510144139/fluent-13-0-lecture06-turbulence-near-wall> (Accessed May 27, 2023).
- 'Ventilateur Centrifuge mobile/chantier, mono/triphasé -Ventilation VIF'. <http://www.ventilation-vif.fr/ventilateur-de-chantier/56-ventilateur-centrifuge-mobile.html> (Accessed October 09, 2022).
- European Council. (2011). Regulation of the European Parliament and of the Council of 9 March 2011 laying down harmonised conditions for the marketing of construction products and repealing Council Directive 89/106/EEC with EEA relevance. *Official Journal of the European Union*, (305), 43–88.
- 'Documents and price lists for energy electricity by Elektro energija'. <https://www.elektro-energija.si/za-dom/dokumenti-in-ceniki> (Accessed October 09, 2022).